

UNIVERSITY OF OKLAHOMA

GRADUATE COLLEGE

ALL-WEATHER SENSE AND AVOID (SAA) RADAR CLUTTER MODELING AND  
CONTROL

A THESIS

SUBMITTED TO THE GRADUATE FACULTY

in partial fulfillment of the requirements for the

Degree of

MASTER OF SCIENCE

By

MATTHEW DAVID GILLIAM

Norman, Oklahoma

2020

ALL-WEATHER SENSE AND AVOID (SAA) RADAR CLUTTER MODELING AND  
CONTROL

A THESIS APPROVED FOR THE  
SCHOOL OF ELECTRICAL AND COMPUTER ENGINEERING

BY THE COMMITTEE CONSISTING OF

Dr. Yan Zhang, Chair

Dr. Justin Metcalf

Dr. Cameron R. Homeyer

© Copyright by MATTHEW DAVID GILLIAM 2020  
All Rights Reserved.

# Contents

Abstract .....	vii
Chapter 1 Introduction .....	1
1.1. Radar Fundamentals Front End .....	1
1.2. Problem Statement .....	4
1.3. Objective of Thesis Research.....	5
Chapter 2 Different Operational Modes for SAA .....	7
2.1 Radar Range Equation .....	7
2.2 Weather Radar Range Equation.....	7
2.3 Radial Speed and Doppler Measurements .....	8
Chapter 3: Airborne Radar Return Modeling with Ground Clutters .....	122
3.1. Ground Cluter Model .....	13
3.1.1 Constant Gamma Clutter Modeling .....	13
3.1.2 Alternative Ground Clutter Models .....	14
3.1.3 Fidelity of the Simulaion .....	14
3.2 Geometries and Parameters of the Flight.....	15
3.3 Modeling of Storm Vertical Profile.....	16
3.3.1 Assumptions.....	16
3.4 Measurement of Ground Clutters with X-band Radar .....	22
Chapter 4: Airborne Radar Processing and Clutter Mitigation.....	27
4.1 Motion Compensation.....	27
4.1.1 Simple Motion Compensation Algorithm .....	27

4.1.2	TACCAR .....	29
4.2	Processing for Moment Data .....	30
4.2.1	Pulse Pair Processing .....	31
4.2.2	Multi-Lag Processing.....	32
4.2.3	Attenuation Correction.....	33
4.2.4	Range Correction, Calibration, and Propagation Loss.....	33
4.3	Moving Target Indicator (MTI) .....	34
4.3.1	Introduction to MTI .....	34
4.3.2	Alternatives to MTI .....	36
4.3.3	Simulation of Basic AMTI .....	37
4.4	Adaptive MTI Filtering .....	43
4.4.1	Algorithm .....	43
4.4.2	Example Results.....	47
4.5	Detection of Turbulence Hazard Through the F-Factor Index .....	48
4.6	Tilt Managment.....	49
4.7	Overall Processing Chain for an ABSAA Radar Operation .....	51
4.7.1	Point Target Channel .....	53
4.7.2	Weather Target Channel .....	53
4.7.3	Results for NASA flight Test Data .....	54
4.8	Motivation and Basic Configuration of Simulation Using NEXRAD Data as Truth Input Field.....	56
4.8.1	Evaluation of Impacts of Different Paramters .....	60
4.8.2	Impact of Clutter Power Levels .....	60

5	Summary, Conclusion and Future Works .....	64
5.1	Summary .....	64
5.2	Conclusion .....	64
4.5	Future Works .....	65
	References .....	67

## **Abstract**

The background of this thesis is related to the enhancement and optimization of the Pulsed-Doppler Radar sensor for the need of Detect and Avoid (DAA), or Sense and Avoid (SAA), for both weather and air-traffic (collision aircraft) detection and monitoring. Such radars are used in both manned and unmanned aircraft for the situation awareness of pilot navigation operations. The particular focus of this study is to develop a simulation model that is based on MATLAB's phased array toolbox and use that simulation model to predict the performance of an end-to-end radar signal processing chain for all-weather, multi-mission DAA. To achieve this goal, we developed an airborne system model based on MATLAB toolboxes, NASA's airborne radar flight test data, and NEXRAD radar data. The measured data from airborne and ground-based radars are used as the "truth field" for the weather. During the modeling and verification process, we primarily investigated the impact of ground or surface clutters on the radar outputs and results, which include the testing of the constant-gamma model using actual measured radar data and improved system and sensor modeling based on the clutter geometry. Evaluation of various moving target indication (MTI) techniques were tested with the simulation model.

## **Chapter 1 Introduction**

---

Modern radars have many diverse functions and as a result require many different designs and algorithms. For instance, an air traffic control (ATC) radar would need to scan the entire airspace, which requires a different design and processing than a synthetic aperture radar (SAR) which is used for imaging. In a weather radar's case, all the targets are distributed over a large area instead of point targets like airplanes. All require drastically different mechanical, electrical, and software designs and processing as well as methods of scanning and solving challenges.

The motivation of this thesis is a special type of airborne radar mission called Detect and Avoid (DAA) or Sense and Avoid (SAA), which is a mission required by unmanned aerial vehicle (UAV) to avoid various types of collision targets (such as non-cooperative air-traffic) and weather hazards [1].

### **1.1 Radar Fundamentals Front End**

A radar transmits an electromagnetic wave at a certain frequency or a range of frequencies and at a certain power. In order to transmit or receive at desired frequencies and power the transmitter and receiver need to be carefully designed. The transmitter chain is responsible for mixing the intermediate frequency to the radio frequency using a local oscillator (LO). Then it amplifies the power to be transmitted by the antenna. In comparison, receiver chain prepares the received signal from the antenna. It amplifies the received signal then mixes the frequency with the LO frequency in the opposite direction converting the received signal to the intermediate frequency (IF). Then the IF will be filtered and converted to digital format by the analog to digital converter (ADC) [2]. The analog part of the radar is referred to as the front end, and the processing of the signal after the ADC is the back end.

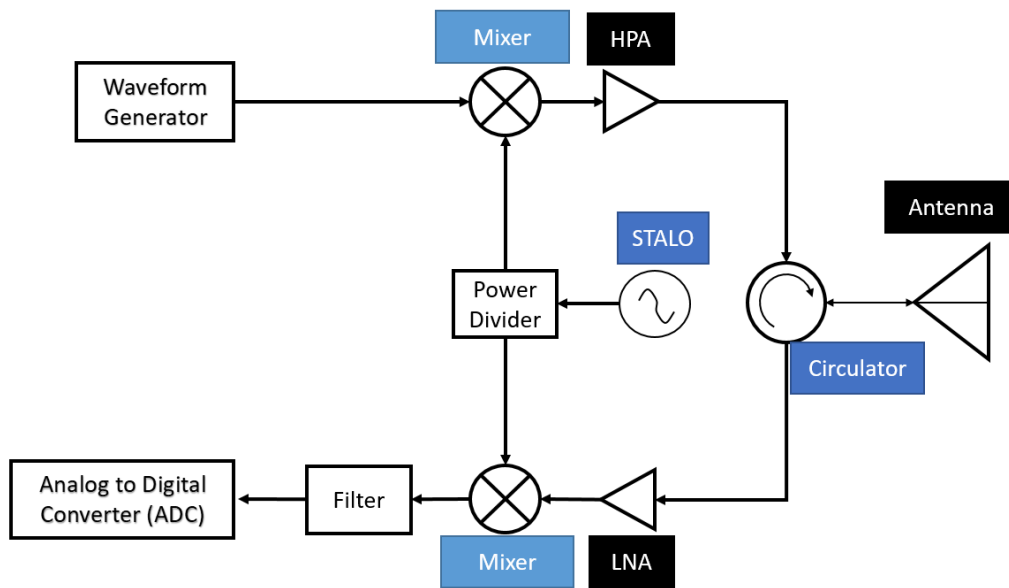


**Figure 1: A basic diagram of a mono-static radar [2]**

Figure 1 shows an example of a basic monostatic pulsed radar receiver. The transmit chain starts with a generated waveform from a coherent oscillator (COHO) that gets mixed with a stable local oscillator (STALO). This brings the frequency up to the desired transmit frequency. Then the power gets amplified by the high power amplifier (HPA). Now the frequency is at the desired power to get sent through the circulator. The circulator is designed to only send one way and receive another. The circulator could be replaced with a switch that works in the same way. Where the transmit and receive signals only get transmitted/received in their respective chains. These two devices protect the components from the power that could be reflected back at a greater power or sent down the wrong chain. For instance, if the signal after the HPA was sent directly to the receiver, it would destroy the low noise amplifier (LNA). Adding a power limiter before the LNA would reduce this risk.

Once the signal is received by the antenna, the signal is sent through the receiver chain. The receiver is responsible for amplifying, filtering and changing the signal to the intermediate frequency. Since the received signal power should be low, a low noise amplifier is used before the mixer. Then the signal is mixed with the LO frequency to convert the frequency the intermediate frequency for the filter and ADC [3]. After the ADC, the signal is processed using different algorithms discussed in future chapters.

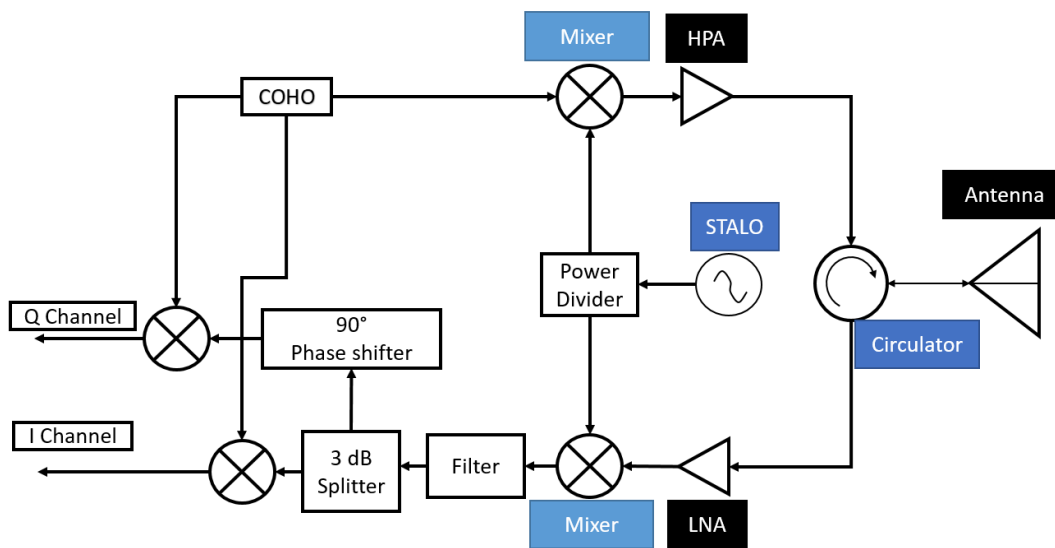


**Figure 2: Mono-Static Radar with I/Q channels [3]**

Airborne radar needs to be able to process the phase of the incoming signal and not just the power return. Measuring the phase will allow the radar to detect positive and negative Doppler speeds. Figure 2 shows the difference in the receiver chain from Figure 1. The main difference is before converting the signal to digital the phase needs to be changed by 90 degrees to create two channels. One channel is quadrature (Q) and the other is in-quadrature (I). These two channels allow for the radar to distinguish between objects moving in a positive or negative direction [3]. This is

extremely important for pilots to determine their new trajectory as well as implementing different radar signal processing strategies.

## 1.2 Problem Statement

If the radar antenna has to point down, there would be ground clutter returns that can greatly distort the velocity and reflectivity estimations, if there is no proper processing to mitigate them. The radar would be pointing downward for reasons such as an aircraft that is at a lower altitude or to properly gauge the power of a storm.

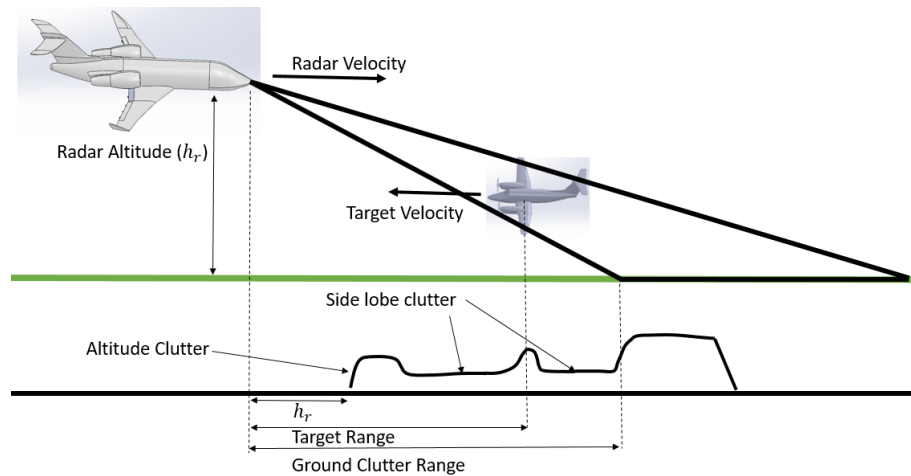


**Figure 3: Example of downward airborne radar clutter for hard target SAA mode**

As shown in Figure 3, there is altitude clutter return and sidelobe clutter, causing further degradation of the radar data quality [4]. The altitude clutter is from the aircraft typically being closer to the ground than the target, so the reflection from the ground is stronger. Sidelobe clutter suppression is a concern for all radars, which is based on the antenna. Fortunately, there are ways to mitigate sidelobes. A few methods are multiple PRF strict timing returns from the ground, and another method is adding another antenna and receive chain that detects the sidelobe return and removes it [4]. Adding another receiver chain would increase the costs of the radar, so adding an

algorithm that can remove the clutter may have cost benefits. Mitigation of these clutter returns is extremely important.

Airborne sense and avoid (ABSAA) for weather and other aircrafts have to work in different ways to address the problem of clutter. There are some methods of detecting aircrafts that would completely remove the weather such as airborne moving target indicator algorithms (AMTI). Whereas leaving the weather alone would reduce the detection of aircrafts. Properly modeling ground clutter to identify the target is crucial for airborne radar.

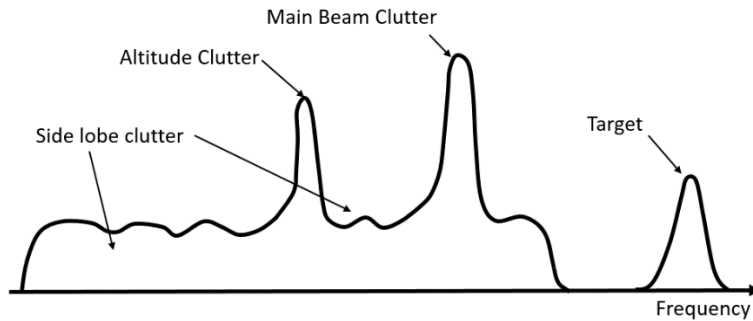


**Figure 4: Doppler frequency clutter [4]**

Figure 4 shows a target and typical clutters in the frequency domain or Doppler spectrum. The sidlobes spread more before the main beam. Since the altitude clutter is due to the sidelobes, it is located somewhere behind the mainbeam as well. Hopefully, the target in question is outside of the clutter region, but this will not always be the case.

### **1.3 The objective of Thesis Research**

The focus of this thesis is to characterize the impact of terrain/ground clutters on airborne radars that are for DAA/SAA operations. The thesis reviews different processing algorithms for AMTI and any potential algorithms that will be useful. Block diagrams of overall processing chains for point and weather targets were developed. In order to validate the signal processing approach for the proposed SAA operation, we developed a novel airborne radar simulator. The

simulator was built from previous works from the phased array simulator (PASIM) in reference [5]. The phased array simulated was a ground based radar simulator that used NEXRAD data to generate simulation scenarios.

The novelty in this thesis is generating an airborne radar DAA mode simulation for any type of weather targets, ground clutter, point target and a combination of targets and clutters for airborne application. The simulator can use measured data from ground based radars and simulate airborne radar observations with different system configurations and platform motions.

Furthermore, full airborne plan position indicators (PPI) images can be simulated from real radar data with the use of NEXRAD. Since NEXRAD stores the entire scene of a storm or weather phenomena, different scenarios for airborne weather radar can be tested.

After the generation of the IQ data, we validated proposed processing strategies with actual measured flight test data provided by NASA Langley Research Center. The data and simulation are only for the weather SAA mode, but can be extended to aircraft SAA mode. Based on the simulation model, we studied and demonstrated the effectiveness of the proposed simple signal processing method for adaptive AMTI filtering.

## Chapter 2 Different Radar Operational Modes for SAA

---

### 2.1 Radar Range Equation

Identifying point targets for aircraft is extremely important to avoid air traffic and a potential collision. A fundamental way that the power return from a point target is estimated is from the radar range equation as shown below

$$P_r = \frac{P_t G_t}{4\pi R^2 l} \times \frac{\sigma}{4\pi R^2 l} \times \frac{G_r \lambda^2}{4\pi l_s} \quad (2.1)$$

$P_t$  = transmit power

$R$  = range to target

$l$  = loss due to propagation

$l_s$  = loss due to receiver

$\sigma$  = radar cross section

$\lambda$  = wavelength

$G_t$  and  $G_r$  = transmit and receiver gain

The first portion of equation 2.1 represents the transmitted power density with the gain of the transmitter and antenna and the propagation loss. Then as the transmitted wave reflects off objects. The power gets reflected back which is represented by the second product of equation 2.1. Finally, the last portion is the receiver with the aperture of the antenna already substituted in.

### 2.2 Weather Radar Range Equation

Sense and avoid for weather is different primarily based on weather being a distributed target than a hard target. As a result of being distributed, the radar range equation must be updated. The RCS is no longer the reflection from a point but the return of a volume. The antenna pattern in azimuth and elevation create an ellipsoidal resolution volume which is defined as follows.

$$\Delta V = \frac{c\tau\pi R^2 \theta_{az} \theta_{el}}{8} \quad (2.2)$$

$\tau$  = pulse width

$\theta_{el}$  = elevation bandwidth

$\theta_{az}$  = azimuth bandwidth

R = range to target    c = propagation speed typically estimated to be the speed of light

The average RCS per unit volume,  $\eta$ , is known as reflectivity, which is given by the next equation.

$$\eta = \frac{\pi^5}{\lambda^4} |K_w|^2 Z \quad (2.3)$$

$\lambda$  = operating wavelength     $K_w$ =dielectric factor of water

$Z$  = reflectivity factor in units of  $mm^6 m^{-3}$

The reflectivity factor is put in terms of decibels, which is  $dBZ = 10 \log_{10} Z$ . The dielectric factor of water can be calculated from the dielectric constant of water:

$$K_w = \frac{e_w - 1}{e_w + 2} \quad e_w = \text{dielectric constant of water} \quad (2.4)$$

The radar Range equation for the distributed target (weather) is now:

$$P_r = \frac{P_t G^2 \lambda^2}{(4\pi)^3 R^4 l_a l_s} \frac{\pi^5}{\lambda^4} |K_w|^2 Z \frac{c\tau\pi R^2 \theta_{az} \theta_{el}}{8} \quad (2.5)$$

Where the  $\sigma$  was replaced by  $\eta \times \Delta V$ . Note that the Rayleigh approximation is acceptable when the hydrometeors are small compared to the wavelength [2]. We can simplify this equation as follows.

$$P_r = \frac{P_t G^2 \pi^3 |K_w|^2 c\tau \theta_{az} \theta_{el}}{512 * R^2 l_a l_s \lambda^2} Z \quad (2.6)$$

Most of the equation above can be stored in a constant which is typically called the radar weather constant. The constants are shown combined in equation 2.8. When equation 2.6 is solved for reflectivity and substituting the constant and attenuation loss values, the equation becomes

$$Z = \frac{P_r R^2}{C L_a} \quad (2.7)$$

$$C = \frac{P_t G^2 \pi^3 |K_w|^2 c \tau \theta_{az} \theta_{el}}{512 * \lambda^2 l_s} \quad (2.8)$$

$L_a$  = total attenuation factor

The constant portion C can be scaled up or down based on different calibration testing. This is due to any potential manufacturing or real-world application differences that are not predicted in theory.

### 2.3 Radial Speed and Doppler Measurements

Doppler frequency change happens when a radar backscatter returns a different frequency back from an object due to its motion. For radar, the frequency change is measured and indicates the target or object's speed.

The Fourier transformation is also used to analyze the frequency shifts. The discrete Fourier transform (DTFT) is used to change the time domain to the frequency domain. This transform is shown in the next equation.

$$Y_s(\omega) = \sum_{m=-\infty}^{\infty} y[m] e^{-i\omega m} \quad \omega \in (-\pi, \pi) \quad (2.7)$$

$Y_s(\omega)$  = frequency function of the Doppler shifts between pulses

$y[m]$  = slow time samples

$\omega$  = a periodic  $2\pi$  radians per sample

There is fast time and slow time when transmitting multiple pulses. The fast time refers to the sampling time as the pulses are transmitted and received. The slow time is the time between each

of the pulses being transmitted. The max speed that can be measured depends on the wavelength and PRF.

$$V_u = \frac{\lambda_0}{4} \times PRF \quad (2.7)$$

$PRF$  = pulse repetition frequency       $\lambda_0$  = operating wavelength

The range of the max unambiguous velocity is  $-V_u$  to  $V_u$ .

The Doppler spectrum can have ambiguities when the target's speed is too high. This causes the observed speed to be at a modulo of the maximum unambiguous speed. For instance, if the speed of the target is 18 meters a second and the max unambiguous speed is 15, the target would look as though it was moving -12 meters a second. In this case, the speed wrapped around to the other side (the negative side) of the spectrum.

This wrapping (or aliasing) can be caused by the motion of the aircraft platform as well. Since the unambiguous velocity and the speed of the plane is known, the aliasing can be cancelled out by subtracting the speed of the plane. This does not correct the aliasing from the speed of the target. More details of these aspects will be discussed in the Chapter 4.

A problem in estimation that may occur when taking the FFT is spectral leakage. Since there is only a finite amount of FFT points representing the frequencies, there will energy from frequencies that are in-between these points. This energy spreads onto neighboring frequency points with decreasing power the farther from the incident frequency point. There are two well-known methods of reducing this problem.

One method is applying a window function. Windowing reduces the power from the discontinuities of the boundaries of each finite sequence [6]. There are many different types of window functions such as rectangular, Hann, Hamming, or Blackman window functions.

The second method of reducing is zero padding the input signal [7]. For instance, there might be 32 pulses in a CPI and an FFT of 1024 points is desired. The 32 pulses get the difference between the points and the pulses added on making it a vector size of 1024 samples (32 pulses plus 992 zeros). Fewer zeros might be just as accurate depending on the application. These two methods will greatly reduce the amount of spectral leakage.

## Chapter 3: Airborne Radar Return Modeling with Ground Clutters

Ground clutter is a special type of distributed target. The existing flight test data from NASA contains airborne weather that can be revealed with some processing. The test data is flying at around 339 meters, but commercial flights are between 9 to 12 km at cruising speed. If they want to have the best estimation of storm magnitudes, they must scan downward in order to cover the storm core, which adds ground clutter. To illustrate the impact of ground clutters on weather avoidance, in Figure 5, radar measurement data from the Next Generation Radar (NEXRAD) was used as truth data for weather and as an example of storm altitudes.

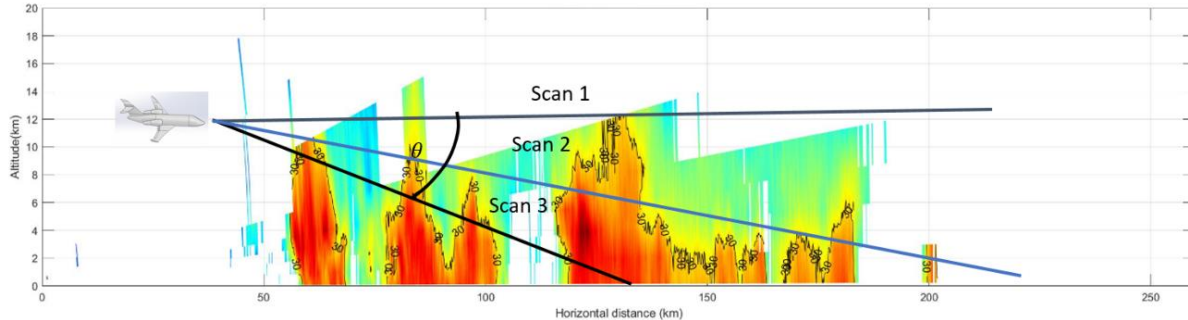


**Figure 5: Geometry of airborne radar scanning and ground coverage**

Scan 1 has a tilt angle, which is too high since the main beam only covers the top of the storm. This misses the near range storm cores as well as the further ones. Scans 2 and 3 have better coverage of the storm cells; however, they are overwhelmed with ground clutter after a certain range. In practice, it is important to pick a specific tilt angle to optimize the cloud measurement while minimizing the return from ground clutter.

## 3.1 Ground Clutter Model

### 3.1.1 Constant Gamma Clutter Model

We used the *Constant Gamma* Clutter Model from MATLAB phased array systems toolbox for clutter generation. The “objects” created from this model allow for a way to add clutter to the phased array simulation. The clutter modeling is based on the following assumptions: the radar system is monostatic; the propagation is in free space; the terrain is homogeneous; the clutter patch is stationary during the coherence time; the spatial response and Doppler shift can be approximated by phase shifts as the radar signal is narrowband; and the radar system maintains a constant height during the simulation flight path [8].

The assumption that the terrain is homogeneous may not always be realistic. For a given PPI, each individual cell’s gamma parameter cannot be changed. However, the gamma value from the constant gamma clutter model can change from cell to cell. How well any given terrain is represented is ultimately limited by the area of each cell. For instance, if a cell contains both flat land and forest, the gamma value should be a value between the two. For our simulations, the clutters are assumed to be one type.

Also, the acquisition of accurate values of specific terrain types might be a laborious and difficult task. Meaning that in order to verify and use gamma value, we would have to go measure the clutters for each type of terrain, which is out of the scope of this paper. The values provided by MATLAB were assumed to be reasonable.

MATLAB has built-in gamma values for many types of landscapes. For example, the terrain types include woods, metropolitan, rugged mountains, farmland, wooded hill, and flatland. The default gamma values are based on 10 GHz radar operating frequency, and for other operating frequencies, the gamma values are calculated by:

$$\gamma = \gamma_0 + 5 \log\left(\frac{f}{f_0}\right) \quad (3.1)$$

$\gamma_0$  = gamma value at 10 GHz     $f$  = operating frequency of simulation

$f_0$  = frequency of the gamma value was generated by default (10 GHz)

### **3.1.2 Alternative ground clutter models**

There are different methods to estimating the backscatter from ground clutter. One example is estimating the ground clutter range/Doppler distribution by its mean power [9]. This method first takes the average power of the random variable at the output of the FFT filter from an elemental scatterer. Then integrates it over the ground surface. After integration, the inputs to the simulation are converted to airborne radar parameters (e.g. aircraft velocity, altitude, PRF) [9]. If someone cannot use the phased array toolbox, the results from this method look promising.

The example is similar to the constant gamma clutter model in terms of how the ground reflectivity is represented. Yet, it gives greater detail on how to represent the range/Doppler spectrum to resemble the distribution of ground clutter with any specific radar antenna and parameters. If the MATLAB's ground clutter function were not already created, this would be a great method of creating the ground clutter.

### **3.1.3 Fidelity of the Simulation**

Multiple sources of errors are expected and can be controlled by trading off with computational loads or measurement workloads for our system simulation. For example, when modeling an antenna radiation pattern, the better the angular sampling resolution, the less interpolation is needed for clutter simulation, and the better the overall clutter simulation accuracies. Unfortunately, for our specific cases, the testing data from NASA's flight tests do not have the

associated antenna patterns, instead, only the gain and sidelobe levels are provided. We then generated simulated antenna patterns base on simplified models, which can be a potential source of errors.

### 3.2 Geometries and Parameters of the Flight

The “truth data” for this system simulation originate from NASA’s airborne radar flight test campaign back in the 1990s. The flight test was mainly for observing wind shear and turbulence using X-band pulsed Doppler radars. The flight geometry and parameters are shown in Figure 6 and Table 1, respectively. The collected flight has for each PPI 128 pulses, 91 range gates, and a range of azimuth angles from 83 to 122.

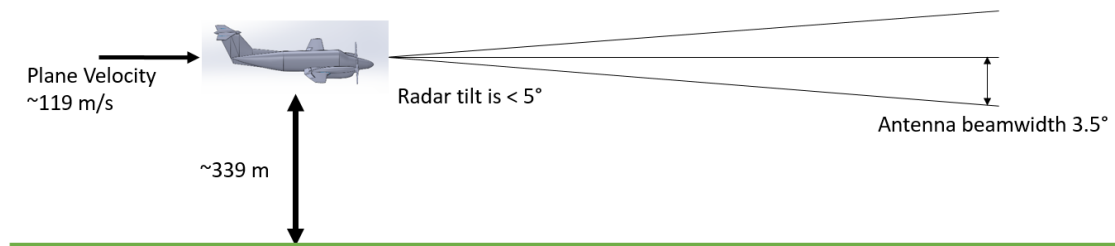


**Figure 6: Geometry of NASA’s flight test data collection.**

**Table 1: NASA Data Flight Parameters [10]**

Radar Parameters	Values	Radar Parameters	Values
Frequency	9.3362 GHz	System noise figure	4 dB
Transmit pulse width	0.96 $\mu$ s	Return signal dynamic range	70 dB
Max radar observation range for flight test	15 km	Receiver dynamic range	100 dB
Transmit PRF	3755 Hz	Xmit/Rec. phase jitter	0.5 d.rms
Range resolution	144 m	Antenna aperture size	0.76 m
Range sampling window	1-10 km	Antenna gain	34.6 dB
Max Unambiguous Velocity	30 m/s	Antenna beamwidth	3.5 deg
Wind speed measurement accuracy	1 m/s	Bin-to-Bin AGC	Applied
Peak Transmit Power	200 watts	Number of A/D conv. Bits	12

One of the objectives is to simulate I/Q data from a similar airborne radar with different antenna tilt angles. This flight test data is used as verification and testing data for processing. It is good to have real airborne data to refer to better match what would be expected for an inflight simulation. As we have discussed from the previous section, the ground clutter return relies heavily on the altitude, tilt/depression angle of the radar and antenna parameters.

### **3.3 Modeling of Storm Vertical Profile**

#### **3.3.1 Assumptions**

Since our intention is to have the capability to simulate airborne radar returns with different antenna tilting angles, a simple model is needed to predict the vertical profile of reflectivity factor for a storm, in order to simulate radar scans for different antenna tilt angles.

Here are the assumptions for the simulations. Firstly, specific terrain type and associated general Gamma values are assumed. Secondly, the weather is assumed to be uniform. At about 340 meters altitude and only 15 kilometers max distance, the weather field is assumed to be constant with regarding to altitude. Therefore, unless the tilt is upwards at a more extreme angle, the reflectivity factor would not change significantly. For lower antenna tilt angle, however, the PPI scan will be increasingly affected by ground clutter return. For instance, at a five-degree depression angle, the main beam reaches the ground at 2.9 kilometers slant range, and the side lobes degrade the radar signals closer than that (assuming flat terrain).

Although this thesis only focuses on low-altitude flight geometry, for more general simulations, aircraft may fly at much higher altitudes than the NASA flight test. For those simulations, NEXRAD radar data was used to explore vertical profiles of radar reflectivity for a typical

thunderstorm. A highly simplified Gaussian curve-fitting is then used to model this vertical profile [11]:

$$y = \sum_{i=1}^n a_i e^{-\left(\frac{x-b_i}{c_i}\right)^2} \quad (3.2)$$

$y$  = fitted vertical reflectivity factor profile based on NEXRAD data

$x$  = the altitude from 0 meters to the max height of the storm

$n$  = number of Gaussian “modes”

$b$  = centroid of the vertical profile

$c$  = width of Gaussian distribution

$a$  = amplitude coefficient

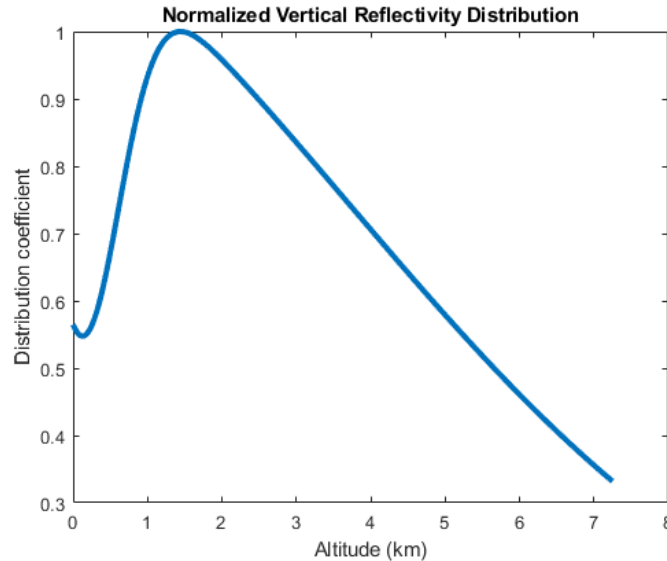


**Figure 7: Normalized Distribution Profile of Radar Reflectivity over Altitudes**

Figure 7 shows an example of vertical profile, which was taken from a tropical storm called Imelda in September 9<sup>th</sup>, 2019. The curve is used to approximate how the reflectivity will change if a different tilt was used than the tilt used in the truth data. Each range bin in a scan will have different altitudes associated with it when the scan is not at zero degrees. The X-axis in Figure 7 are these altitudes. Then the curve can be used to simulate the change in reflectivity factor values for different altitudes. The “truth data” profile would be assumed to be located at the peak of the curve.

The data was manipulated by Py-ART's grid python toolbox [12] . This code interpolates all the ground weather radar's elevation scans and creates a Cartesian grid with a specified latitude, longitude and elevation resolution. The highest reflectivity was used to determine the storms core. Then all the elevation data points from that longitude and latitude position were fitted with the Gaussian distribution from equation 3.2. The distribution has great variability with different storms, which can expand the original data for separate simulation scenarios.

There is one issue that needs to be addressed when simulating weather/air-traffic target returns from different antenna tilt, which is illustrated in Figure 8. Basically, targets located at the same earth-centered horizontal coordinates would map to different range bins of radar scans with different tilt angles. Therefore, larger tilt angle makes the target appear to be further away. This effect can be easily corrected in the signal processing chain. At lower magnitudes of tilt, this effect is negligible.

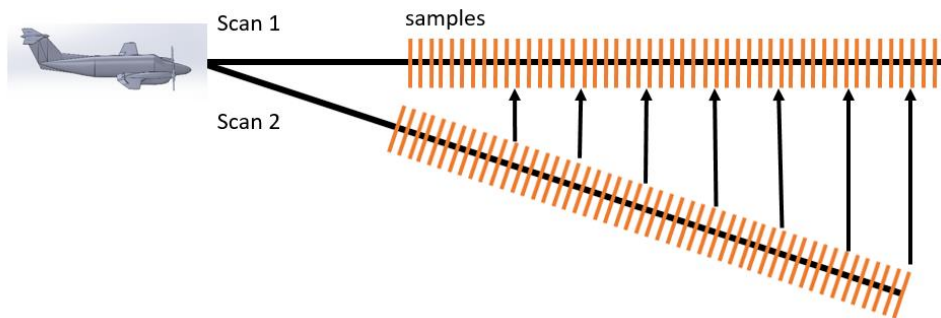
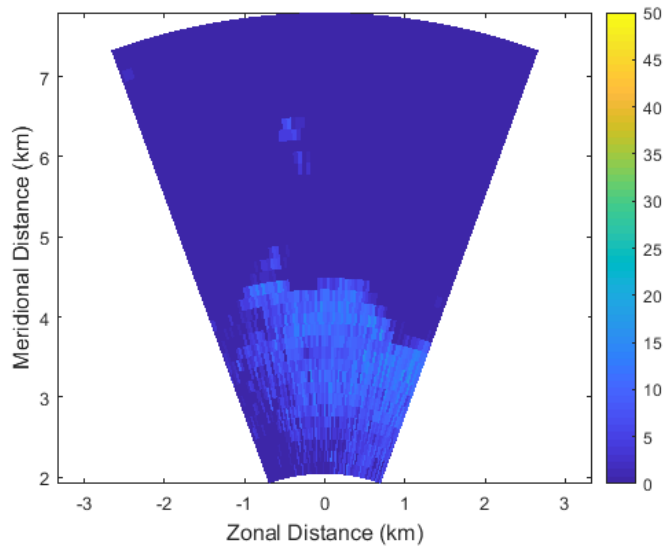
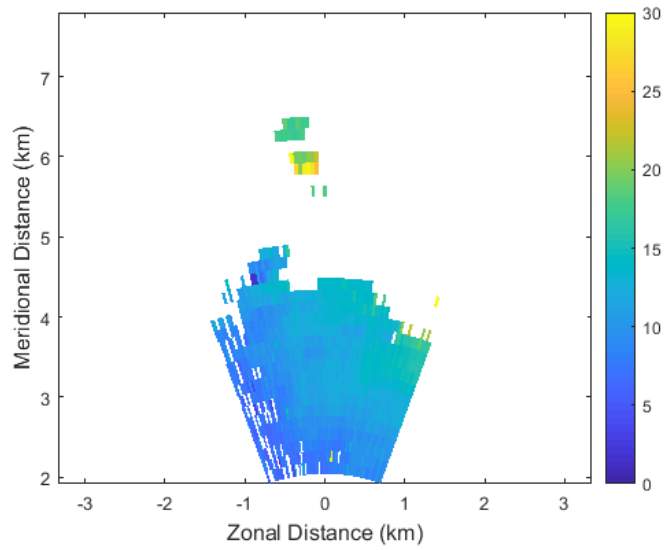


**Figure 8: An illustration of range bin shifting of distributed target for different tilt angles of radar antenna.**

Figures 9 and 10 illustrate the simulated airborne radar returns with clutter impacts. Figure 9 shows the “truth” data without ground clutters, which are based on one of the PPI scans (frame#15 from airborne radar data collection) from actual flight test.



(a)



(b)

**Figure 9: “Truth” airborne weather radar variables from NASA’s flight test data set, frame#30. (a) Reflectivity with constant based on radar range equation, (b) Radial velocity magnitude. An MTI filter was used to remove ground.**

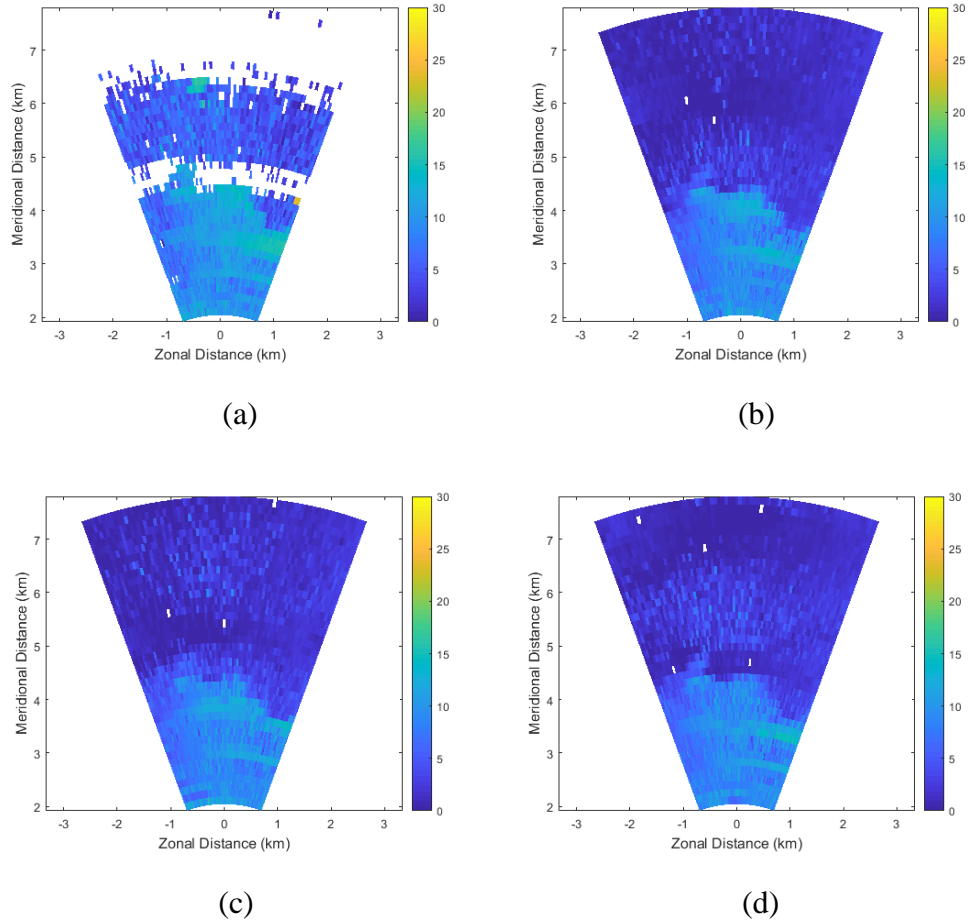


**Figure 10: Effects of ground clutter on magnitude of radial velocity estimations, when the radar antenna has different tilt angles. Tilt angle is 0 at the horizontal altitude line of the aircraft and positive downward looking, (a) has a tilt of  $-1^\circ$  with a threshold removing noise, (b) has a tilt of  $1^\circ$ ; revealing Doppler aliasing, (c) has a tilt of  $2^\circ$ , which causes further degradation, (d) has a tilt of  $3^\circ$**

The sidelobe clutter has a significant effect on the radial velocity estimation, which is illustrated in Figure 10. Because sidelobes point to different spatial directions, radial velocity components caused by them become uncertain. Overall, they cause significant errors in the radial velocity estimation for airborne radar measurements.

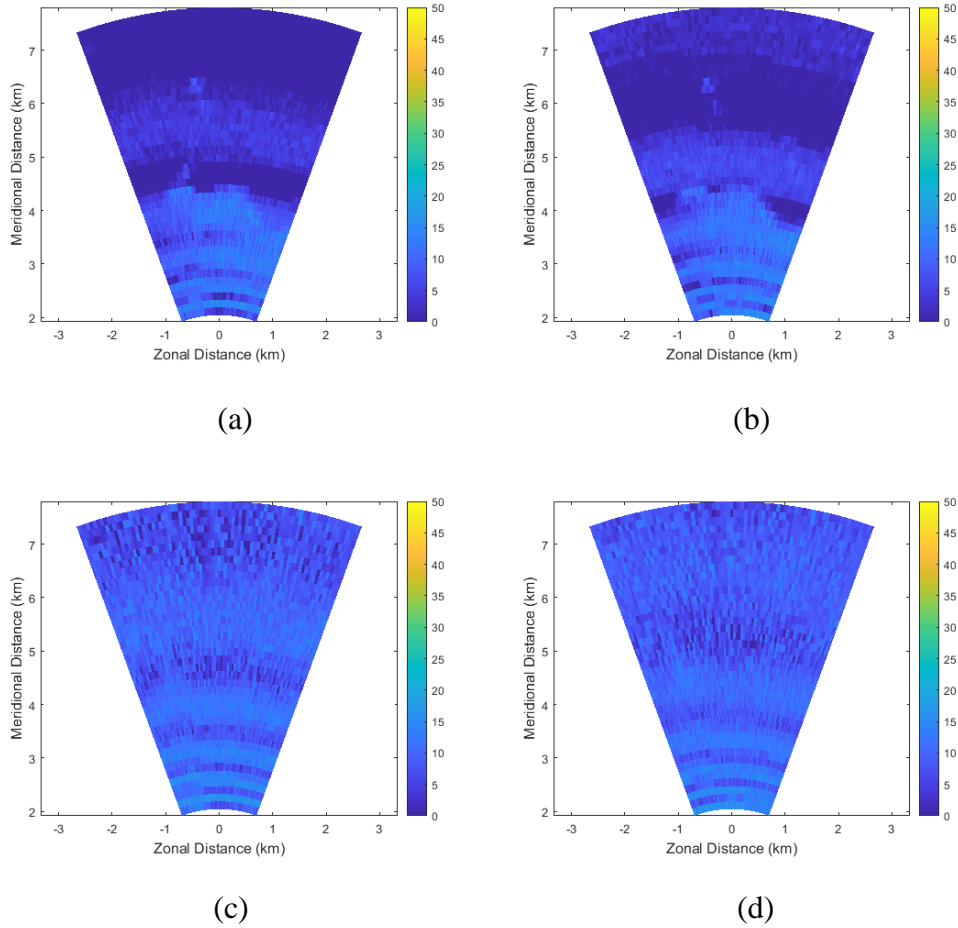


**Figure 11: Effects of ground clutter and different tilt angles on radar raw return power. Tilt angle is  $0^\circ$  at the horizontal altitude line of the aircraft and positive, downward-looking, (a) has a tilt of  $-1^\circ$ , (b) has a tilt of  $0^\circ$ , (c) has tilt of  $1^\circ$ , (d) has tilt of  $2^\circ$ .**

When the radar antenna tilts away from the surface of the earth, the effect of ground clutter is less significant. Figure 11 shows the simulated PPI return of weather return power as results from different antenna tilt angles. In Figure 11 (b) and Figure 11 (c), we can observe the gradual increase of the effects from the main beam clutter. At very low tilt angles, the range bins of a scan may pass the ground interception point so that any range profiles beyond that point are no longer useful.

### 3.4 Measurement of Ground Clutters with X-band Radar

In order to further validate and calibrate the airborne radar ground clutter models, we used Garmin's GWX-70 radar to perform a series of ground measurement tests. The experiment was setup on top of the National Weather Center (NWC) building. The measurement setup is shown in the following Figure 12.



**Figure 12: The measurement setup at NWC roof.**

The GWX radar was setup on a tripod and balanced with a surface level. Then measurements of range profiles were taken from 21 degrees to about -30 degrees elevation angles (the positive

elevation is upwards). The NWC building is 30 meters in height and the tripod is about 1 meter. In total the height is 31 meters. Range profiles from multiple azimuth angles were scanned, primarily pointing north and northwest directions.

Since the radar scene is mainly an urban area and the height of antenna is relative low, the scattering of buildings are more pronounced. Below is an example of the range versus power at elevation angle zero.

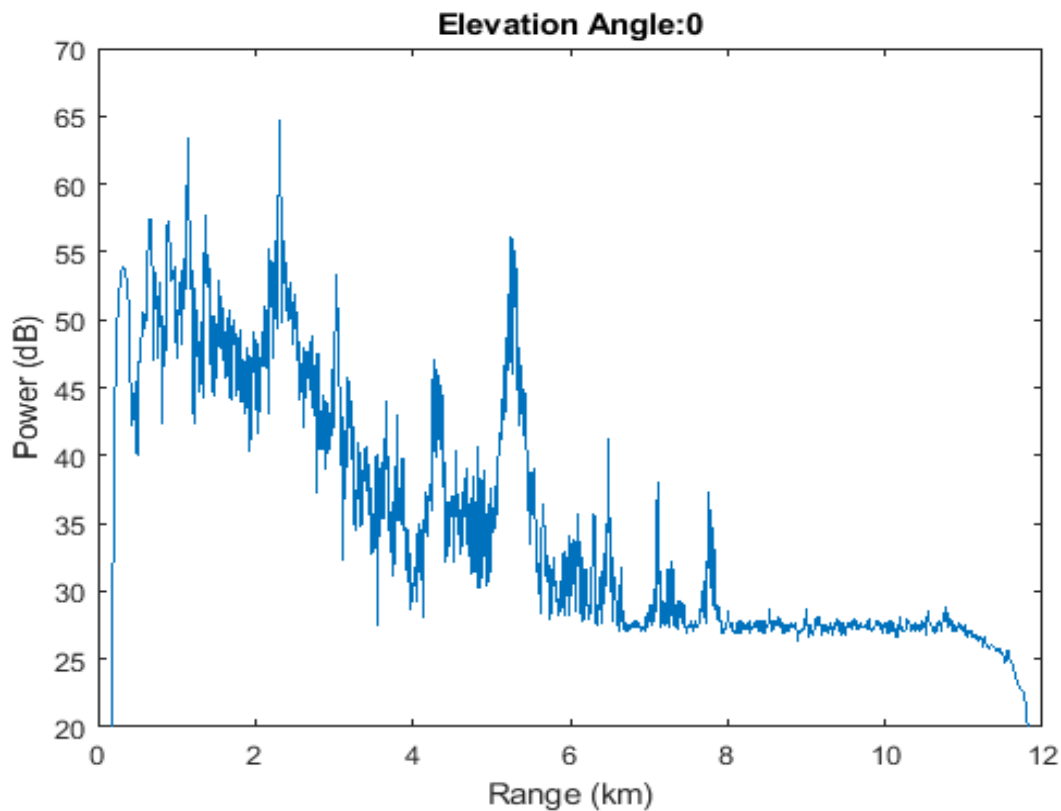


**Figure 13: A sample range profile of ground clutter collected using GWX radar.**

The sharp peaks of Figure 13 is part of the ground clutter returns, such as buildings and water towers. We collected radar signal returns from all the clutter region. Next we computed the

averaged return power across all the range bins, then compared the averaged curve with prediction from constant-gamma model.

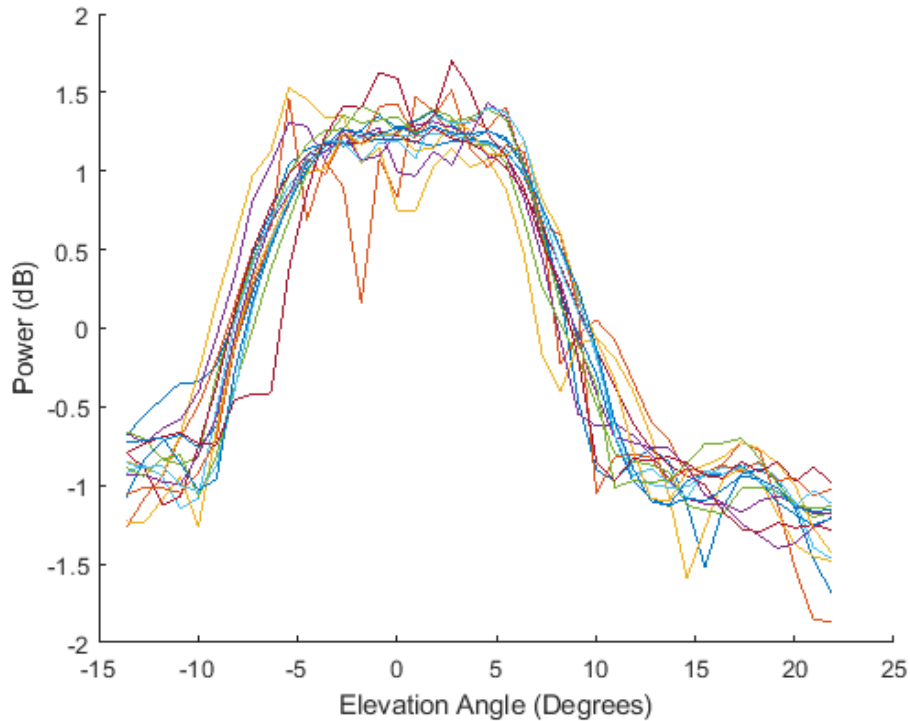


**Figure 14: Normalized GWX ground clutters from sample range bins for different antenna tilt/elevation angles.**

In Figure 14, each line represents return power from a different range bin as the elevation changes. This trend is what the simulation is mimicking. The specific power of the ground clutter will be dependent on the radar configurations, but the trend over elevation or tilt angle is similar.

For the constant gamma clutter model, the power reflected by the ground changes with elevation angle (also known as the grazing angle). The constant gamma model as follows [13].

$$\sigma^0 = \gamma \sin \varphi \quad (3.3)$$

$\gamma$  = estimated ground clutter coefficient

$\varphi$  = grazing angle

The  $\gamma$  value can be scaled to different types of terrain. Table 2 shows some of typical gamma clutter coefficients for different types of clutter [13].

**Table 2: Constant Gamma Clutter Coefficients**  
*Terrain Types*     $\gamma$  (dB)

<i>Mountains</i>	-5
<i>Urban</i>	-5
<i>Wooded Hills</i>	-10
<i>Rolling Hills</i>	-12
<i>Farmland, Desert</i>	-15
<i>Flatland</i>	-20
<i>Smooth Surface, Road</i>	-25

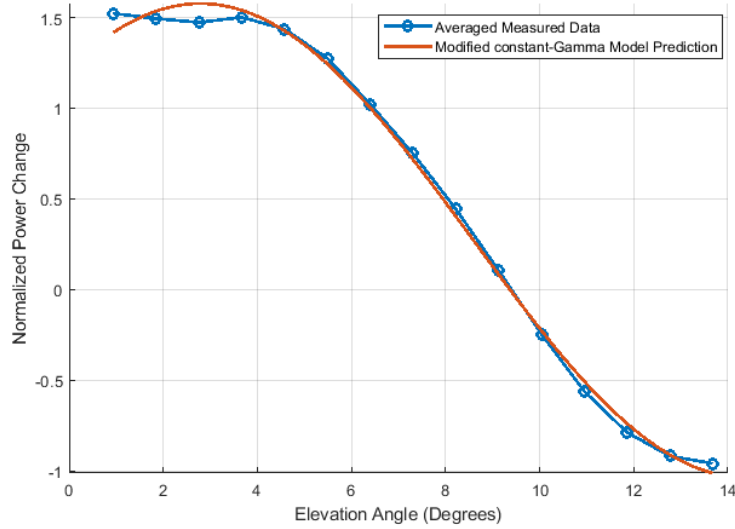


**Figure 15: Comparison between measured clutter return power using X-band radar, and model predicted using constant-gamma model. The curves are normalized return power vs antenna tilt angles (positive tilt angle represents tiling up).**

The sine approximation, used in Figure 15, is a manipulated version of the constant gamma clutter model equation (3.4). The data points were fitted to the following equation using a least-squares cost method.

$$y(x) = b_1 \sin(2\pi b_2 x + 2\pi b_3) + b_4 \quad (3.4)$$

The results of the fit for the dataset in Figure 15 are  $b_1 = 1.3$ ,  $b_2 = -1.043$ ,  $b_3 = -1.63$ , and  $b_4 = .2694$ . The fitted curve shows a similar trend to the constant gamma clutter model.

## Chapter 4: Airborne Radar Processing and Clutter Mitigation

---

In this chapter, we provide details on the algorithms and processing to perform weather and hard-target detection, which is used for All-Weather Sense and Avoidance mission. The simulation model produced from the previous chapter is used. The emphasis is again on the mitigation of ground clutter impacts through basic signal processing.

### 4.1 Motion compensation

#### 4.1.1 Simple Motion compensation algorithm

Platform Motion Compensation (PMC) is required for airborne radars to estimate velocities correctly. Compensation of the ground speed is needed while the plane's roll and pitch were not described in the NASA's data. In our simulated processing chain, the removal of impacts from aircraft ground speed is based on the following equation.

$$v = v_o + 2v_u - \text{mod} \left[ \frac{v_a}{2v_u} \right] \quad v_o < v_u \quad (4.1)$$

$$v = v_o - \text{mod} \left[ \frac{v_a}{2v_u} \right] \quad v_o \geq v_u \quad (4.2)$$

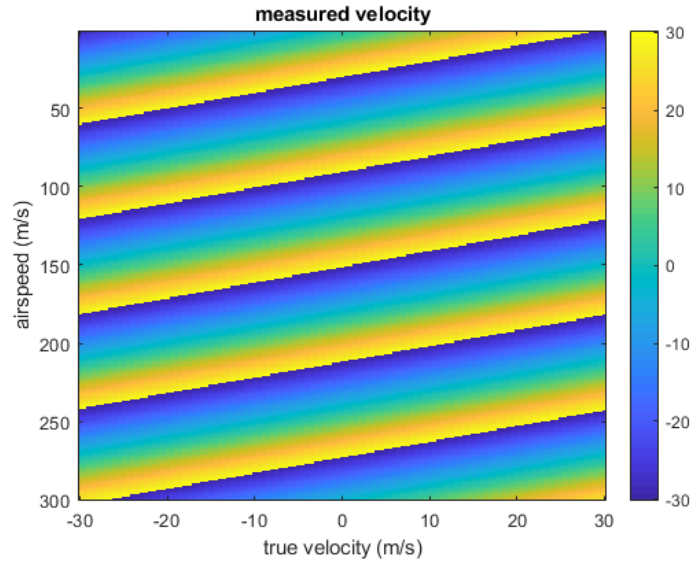
$$v_u = \frac{\lambda \times PRF}{4} \quad (4.3)$$

$v$  = motion-compensated aircraft speed

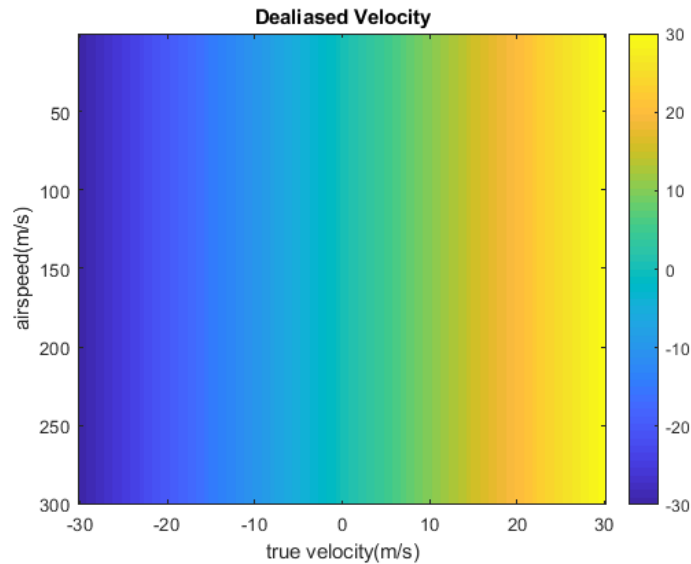
$v_o$  = observed target speed from radar I/Q return

$v_a$  = radar platform velocity

$v_u$  = unambiguous velocity



(a)



(b)

**Figure 16: (a) Measured/Aliased target velocity values based on different true velocities and airspeeds. (b) Output of idealized velocities after the algorithm in equation (3.1) is applied.**

The application of equation (3.1) is illustrated in Figure 16. In Figure 16(a), the measured, or aliased target velocities are plotted in different colors, regarding both true velocities and airspeeds. In Figure 16(b), the compensation/de-aliasing results using equation (3.1) are presented. Equation

(3.1) does not wrap the velocity at this step in our processing. That is why there is a  $2v_u$  added to the observed target speed when  $v_o < v_u$ . If the algorithm rotates the PSD vector like “*circshift*” in MATLAB, then the  $2v_u$  may not be necessary.

In the simulation evaluations, the aircraft is assumed to have near zero pitch and roll, which allows us to avoid the use of a pitch/roll antenna stabilization algorithm. A more rigorous antenna stabilization algorithm is based on the following relation [3]:

$$\begin{bmatrix} i_s \\ j_s \\ k_s \end{bmatrix} = \begin{bmatrix} \cos \theta & -\sin \theta & 0 \\ \sin \theta & \cos \theta & 0 \\ 0 & 0 & 1 \end{bmatrix} \begin{bmatrix} \cos \epsilon & 0 & \sin \epsilon \\ 0 & 1 & 1 \\ -\sin \epsilon & 0 & \cos \epsilon \end{bmatrix} \begin{bmatrix} 1 \\ 0 \\ 0 \end{bmatrix} \quad (4.4)$$

Here,  $i_s, j_s, k_s$  = the horizontal coordinate pointing forward from the plane (positive forward), positive in the direction of the starboard wing, vertical coordinate (positive downward)

$\theta$  = azimuth pointing angle of the radar antenna LOS

$\epsilon$  = elevation pointing angle of the radar antenna LOS

Equation (4.1) should be used to create a stabilized coordinate system with a horizontal and forward-looking scan.

#### 4.1.2 TACCAR

Time-averaged-clutter coherent radar (TACCAR) shifts the clutter in the Doppler power spectrum close to the same amount as the platform so that a simple MTI filter could be used. The clutter return is used to phase lock the radar to the clutter filter or the MTI filters [14].

However, the traditional method of TACCAR has drawbacks. It requires a certain time delay interval for estimation and an analog COHO channel for the mean Doppler frequency of the clutter [15]. Since we have DSP based Doppler FFT processing, we can do this all-digital to avoid using

another analog COHO channel. A method to reduce time delay drawback would be to make Doppler corrections at more than one point [16]. Using a dwell-time based clutter lock MTD within the antenna beam dwell time could be a better approach [15]. This method would break up the CPI into a different section with different motion corrections similar to the suggestion from [16].

A simple version of motion compensation is implemented in our processing with the intention of adding a more complex version in the future.

## 4.2 Processing for Moment data

### 4.2.1 Pulse Pair Processing (PPP)

Pulse pair processing (PPP) is commonly used to process weather return signals. In the slow time power spectrum, PPP assumes that there is only noise and an approximate Gaussian-shaped peak. Therefore, any other clutters should be removed before this processing such as MTI, tilting schemes, etc. The Power, mean Doppler shift, and spectral width are estimated from the shape's amplitude, mean and standard deviation. The autocorrelation function (ACF), shown in equation 4.5, is key in deriving PPP. Where slow-time data is  $y[m]$  with 'm' pulses [17].

$$S_y[k] = \sum_{m=0}^{M-k-1} y[m]y^*[m+k] \quad m = 0, \dots, M-1 \quad (4.5)$$

In order to get the power return, use the peak of the autocorrelation function 4.5.

$$P_y = \frac{1}{M} \sum_{m=0}^{M-1} |y[m]|^2 \quad m = 0, \dots, M-1 \quad (4.6)$$

One can see that after squaring and getting the magnitude of the IQ data, an averaging of the pulses over all the samples in slow time occurs. To get the frequency shift, take the first autocorrelation

lag in equation 4.5 and use it for equation 4.6. In [17], it is shown that the full autocorrelation does not have to be calculated. Only  $y[m]y^*[m + 1]$  would need to be calculated using two slow time samples.

$$\hat{F}_0 = \frac{-1}{2\pi T} \arg(S_y[1]) \quad (4.5)$$

$T =$  pulse repetition time

To convert the calculated frequency shift to velocity multiply by half the wavelength. For spectrum width it is assumed that the Doppler power spectrum has a Gaussian shape with the standard deviation ( $\sigma_F$ ). The spectrum width can be calculated by the following equation and is derived in [17].

$$\hat{\sigma}_F^2 = -\frac{1}{2\pi^2 T^2} \ln \frac{S_y[1]}{S_y[0]} = -\frac{1}{2\pi^2 T^2} \left( 1 - \frac{S_y[0]}{S_y[1]} \right) \quad (4.6)$$

Equation 4.6 uses the approximation of  $\ln x = 1 - \frac{1}{x}$ . A more in-depth derivation of the time-domain and frequency domain PPP estimators is available from reference [17].

### 4.2.2 Multi-Lag Processing

Multi-lag processing uses different correlation estimates from the ACF at multiple lags. As mentioned, when using lag-0 for PPP, it is assumed that the power spectrum density returns only a Gaussian spectrum peak and noise. Using multiple lags can help reduce the noise. Lag 1, lag 1-2 and lag 1-4 power and spectral width are shown below respectively [18].

$$\hat{P}_y = \widehat{S}_y[1] \quad (4.7)$$

$$\hat{P}_y = \frac{|\hat{S}_y[1]|^{\frac{4}{3}}}{|\hat{S}_y[2]|^{\frac{1}{3}}} \quad (4.8)$$

$$\hat{P}_y = \frac{|\hat{S}_y[1]|^{\frac{54}{86}} \cdot |\hat{S}_y[2]|^{\frac{39}{86}} \cdot |\hat{S}_y[3]|^{\frac{14}{86}}}{|\hat{S}_y[4]|^{\frac{21}{86}}} \quad (4.9)$$

$$\hat{\sigma}_v = \frac{\lambda}{\sqrt{24\pi T}} \sqrt{|\ln|\hat{S}_y[1]|| - |\ln|\hat{S}_y[2]||} \quad (4.10)$$

$$\hat{\sigma}_v = \frac{\lambda}{28\pi T} \sqrt{11|\ln|\hat{S}_y[1]|| + 2|\ln|\hat{S}_y[2]|| - 13|\ln|\hat{S}_y[3]||} \quad (4.11)$$

$$\hat{\sigma}_v = \frac{\lambda}{4\sqrt{129}\pi T} \sqrt{\begin{matrix} 13|\ln|\hat{S}_y[1]|| + 7|\ln|\hat{S}_y[2]|| \\ - 3|\ln|\hat{S}_y[3]|| - 17|\ln|\hat{S}_y[4]|| \end{matrix}} \quad (4.12)$$

$\hat{\sigma}_v$  = the spectrum width in terms of velocity

These equations are produced from manipulating the expected ACF then solving the differential function for both power and spectrum width using the least square function. Further explanation is in reference [18].

The computational load for the later lags may cause some problems for real-time radars. “The multi-lag estimator produces moment estimates with smaller bias and standard deviation than conventional estimators when the spectrum width is small” [18]. This requires a more dynamic algorithm of choosing which lags to use for best estimations based on SNR and spectrum width.

The narrower the spectrum width gets the later lags should be used.

### 4.2.3 Attenuation Correction

As the transmitted wave propagates through clouds the water particles will absorb some of the power causing attenuation. A simplified approach to determine the attenuation is used in this thesis. The attenuation is determined by the operating frequency and the reflectivity. The attenuation can be estimated by using a Single Cell Monte Carlo (SCMC) simulation for droplets of water at a particular operating frequency. A scatter plot is generated. Then a power-law relationship curve fit was applied between the attenuation and reflectivity ( $\text{mm}^6\text{mm}^{-3}$ ) to it shown in equation 4.13.

$$A = aZ^b \quad (4.13)$$

A = attenuation factor (dB/km)      a and b = determined by the curve fit

Z = reflectivity ( $\text{mm}^6\text{mm}^{-3}$ )

Attenuation only effects cells with significant water particles in them, so adding a minimum reflectivity threshold is needed. Now that we have an estimate for attenuation the path integrated attenuation (PIA) must be applied for each range

$$PIA(r_k) = 2 \sum_{i=1}^k A(r_i) \Delta r \quad (4.14)$$

$\Delta r$  = range resolution       $r_k$  = the kth range bin

#### 4.2.4 Range Correction, Calibration, and Propagation Loss

Range correction, calibration, propagation loss and attenuation are all represented in the equation 2.7. The range correction and calibration are R and C. Then the propagation loss and attenuation are represented in the L.

The calibration can be measured or calculated as shown in equation 2.8. Measuring the calibration constant might be more reliable in the field to account for variability of the radar. However for airborne weather radar can be difficult to get a good target to calibrate with. For instance if the radar is being calibrated to show relatively the same levels as nexrad measurements, the radar would need to measure the same cloud coverage at the same time.

Propagation loss is dependent on altitude and distance measured because its dependent on the atmospheric pressure. This means that the altitude of each range bin will determine this. If it is assumed that each range bin is on the same altitude then a single value will suffice. For every kilometer traveled by the wave it loses a certain amount of power. For instance, the propagation loss will be in units of dB/km. Charts that depict these values can be found in Scholnik's Radar Handbook.

## **4.3 Moving Target Indicator (MTI)**

### **4.3.1 Introduction to MTI**

The moving target indicator (MTI) is basically a high pass or notched filter that removes the radar returns from objects that are not moving or moving slowly, such as ground clutter returns. It is one of the oldest methods for airborne radar clutter mitigation, while it is still very important for the specific radar we use for the mission. It has good performance for removing weather echo when the objective is to detect point targets like aircrafts, it is also used in our mission to remove ground clutters from useful weather radar return signals. The basic concept for MTI for the airborne radar operation is illustrated in Figure 17.

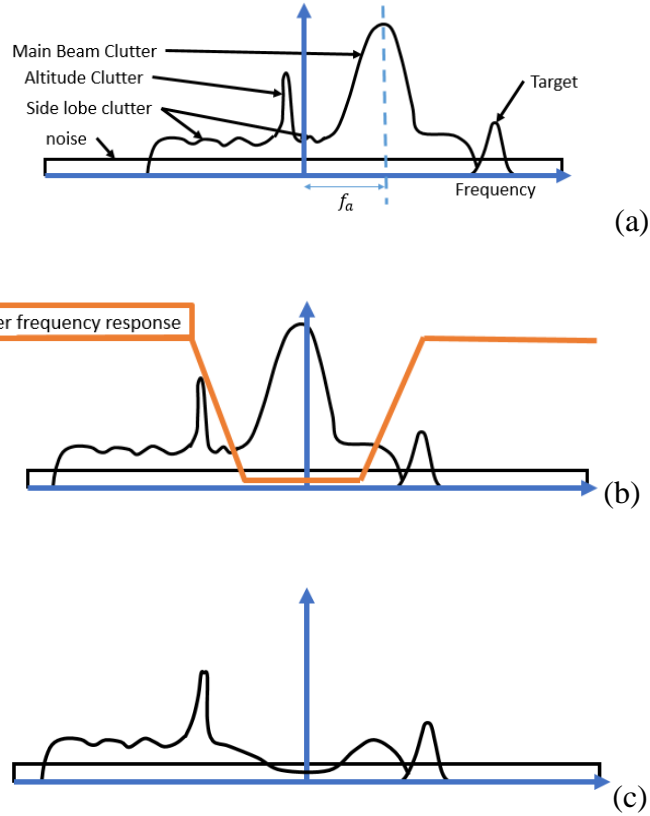


**Figure 17: The basic concept of airborne MTI processing. (a) is the Doppler power spectrum (DPS) with no processing. (b) is motion compensated and is showing a possible MTI filter response. (c) is the resultant Doppler spectrum after the filtering.**

In order to quantify the effectiveness of the MTI filter on clutter mitigation, improvement factor (IF) is defined as the signal to clutter ratio (SCR) after the filter divided by the SCR before the filtering:

$$IF = \frac{\left(\frac{S_o}{C_o}\right)}{\left(\frac{S_i}{C_i}\right)} \quad (4.15)$$

$IF$  = Improvement factor

$C_o$  and  $C_i$  = Clutter power output and input of filter

$S_o$  and  $S_i$  = Signal power output and input of filter

Another method of calculating the improvement factor is to start with clutter attenuation. This attenuation is defined in equation 4.5 as the ratio of MTI filter input clutter power to the output clutter power.

$$CA = \frac{C_i}{C_o} \quad (4.16)$$

$C_i$  = input clutter power to the filter       $C_o$  = output clutter power to the filter

CA = clutter attenuation

Equation 4.6 can be used to rewrite equation 4.5 for the improvement factor.

$$IF = \frac{S_o}{S_i} CA \quad (4.17)$$

For point targets, the filter response can hinder some velocities that have velocities in the filter's notch. Figure 18 shows the frequency response of a 3-pulse canceller. The frequencies that are nulls in the figure would be blind spots. Furthermore, all the frequencies around those areas would be hindered.

### 4.3.2 Alternatives to MTI

There are alternatives to MTI that may improve the airborne clutter mitigation performance, depending on the hardware and application. Some examples are space-time adaptive processing (STAP), adaptive frequency domain set-zero method, and the displaced phased center antenna (DPCA) [14]. Since we only focus on mechanical scanning and low-cost commercial airborne radars in this work, detailed studies and implementations of these methods are beyond the scope of this thesis, but an overview of them is given as follows.

STAP is primarily used to remove clutter in the main beam. It is used for radars with array antennas, which outputs a data cube. The data cube consists of number of pulses by number of

channels (the array) by range samples. A part of its implementation is to apply an FFT between the channels and another FFT to the pulses for each range bin or range sample. Alternatively, a two-dimensional FFT would achieve the same thing to the data cube. Then covariance matrixes are used to compute an optimal filter for ground clutter. STAP was not used in our simulation studies, because in order to use STAP there must be a phased array antenna or multiple phase centers. The adaptive domain set zero method is used to set the Doppler filters to zero when clutter is apparent [19]. Potentially the same process of identifying clutter would be used as in the simplified adaptive filtering approach to be discussed in the next section.

DPCA is a method of motion control that utilizes a long broadside antenna array, where the transmit signal shifts down the aircraft near the speed of the aircraft [20]. From the point of view of the radar, the clutter appears to not shift [20]. This could allow basic MTI methods to be used, such as the two-pulse or three-pulse canceller. However, the type of antenna used is not meant for SAA, yet still deserves mention.

### **4.3.3 Simulation of Basic AMTI**

Figure 17 (a) shows the Doppler spectrum/signal power spectrum of a hypothetical airborne SAA radar signal. As expected, the target Doppler frequency is shifted by the aircraft's speed, which needs to be compensated. The result after motion compensation is shown in Figure 17 (b). MTI filter is then applied as shown in Figure 17 (c). Notice that there is still altitude clutter and sidelobe clutter present after the initial MTI processing. The clutter need to be removed by other means.

The blind regions of the filter can be reduced by staggering PRFs. When staggering PRFs, there will still be sections of the filter response that perform worse. However, the staggering method is considered the most effective way to deal with blind speeds. A staggered PRF example was shown

from MATLAB's MTI example and a variation is presented in Figure 18 and Figure 19 [21]. The targets are at 1600 and 2900 meters. One is traveling at speed outside of the blind speed and the other is traveling at the blind speed. The PRFs are 25 kHz and 30 kHz, respectively. As shown in the figure, the noise is no longer based on the range but the receiver noise floor.

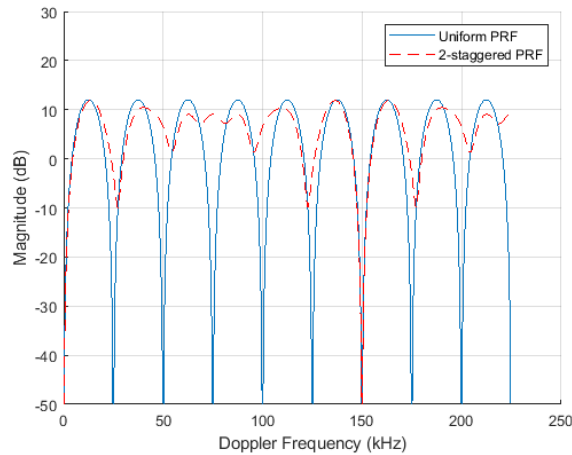


**Figure 18: Frequency response of a 3-pulse canceller with uniform PRF and a staggered PRF.**

Without PRF staggering the second target is invisible to the radar. It is important to choose the right filter with staggering PRFs when designing an MTI algorithm.

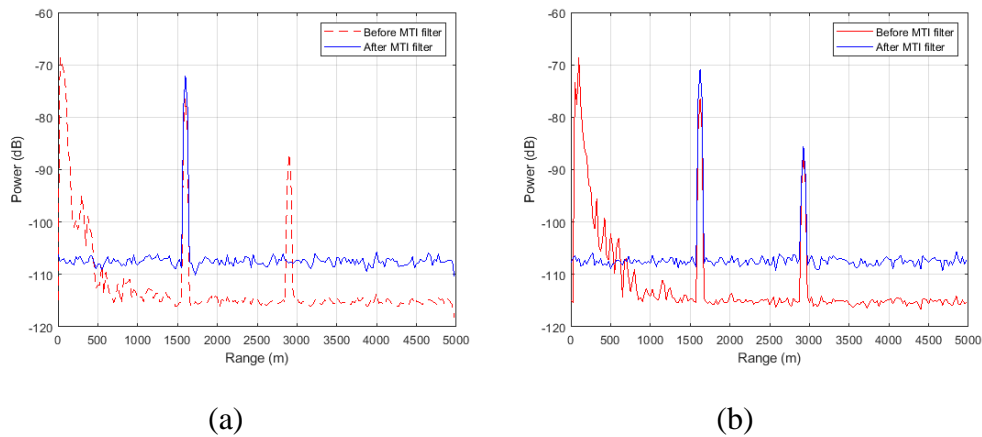


**Figure 19: Power versus range plots for a radar. (a) is power versus range plot with only the 3-pulse canceller and (b) is power versus range plot with MTI staggering**

There are many ways to stagger different PRFs. An algorithm can transmit all the pulses for a PRF in a burst then switch to the next PRF or stagger them switching from one PRF to the next every pulse with a set number of pulses per PRF. Another method could be switching between PRFs randomly. Through careful selection of a cost function, the best method was shown to be a simple burst mode where all the pulses for one PRF is transmitted before transmitting the next PRF [22].

As an initial experiment, we simulated the airborne radar system operation and data output by combining the NASA’s flight measurement data and the modified constant-Gamma clutter model. The simulation parameters and geometries are described in Table 1 of Section 3.4, and the specific weather is a convective storm. We first tested the dual-pulse canceller as the simplest form of MTI processing.

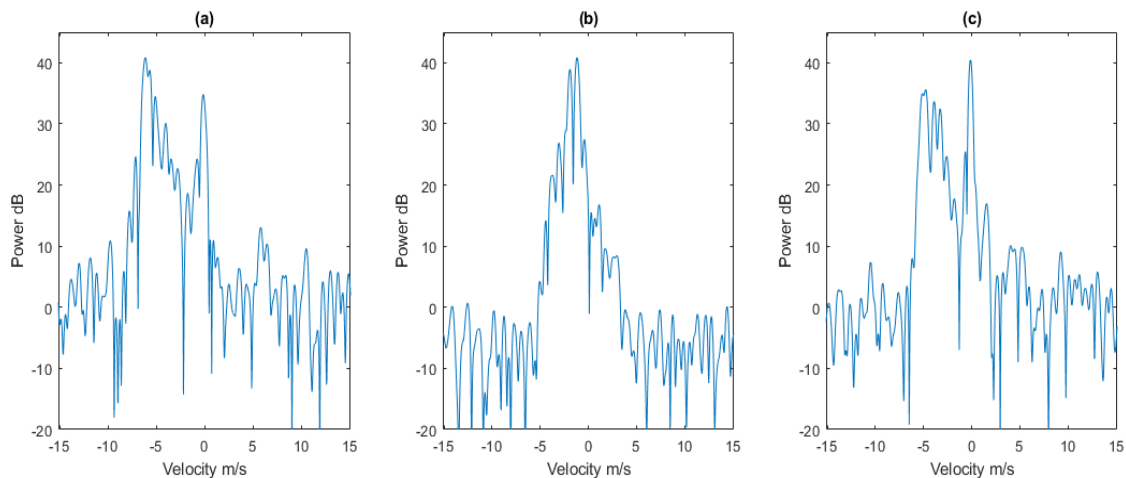


**Figure 19: Doppler power spectrum of the sample flight test data. a) shows the weather has higher power levels (left peak) than the ground (peak at 0 m/s); b) shows weather and ground powers mixed; c) shows a case that ground clutter has greater power than that of weather return.**

The plots within Figure 19 show the Doppler spectrum of three different range bins for one azimuth scan from frame #30 of the NASA data. They represent different possibilities of relative power levels between weather return and ground clutter. Note that for these example data, the ground

clutters show up at almost zero Doppler. This is simply due to the choice of PRF verses speed that purposely puts the “aliased clutter return” at near zero Doppler frequencies. In this case, if the unambiguous velocity and speed are divisible by each other the ground return would seem to be at zero. For Figure 19 (b) and (c), the power return from the ground clutter causes these range bins to have a peak near zero-Doppler. It is needed to determine which portions near zero Doppler are ground clutter or weather.

The outputs from a simple two-pulse canceller for these sample cases are shown in the following sample (Figure 20). A 2-pulse canceller is a simple FIR filter that has a transform function of  $H(z) = 1 - z^{-1}$ .

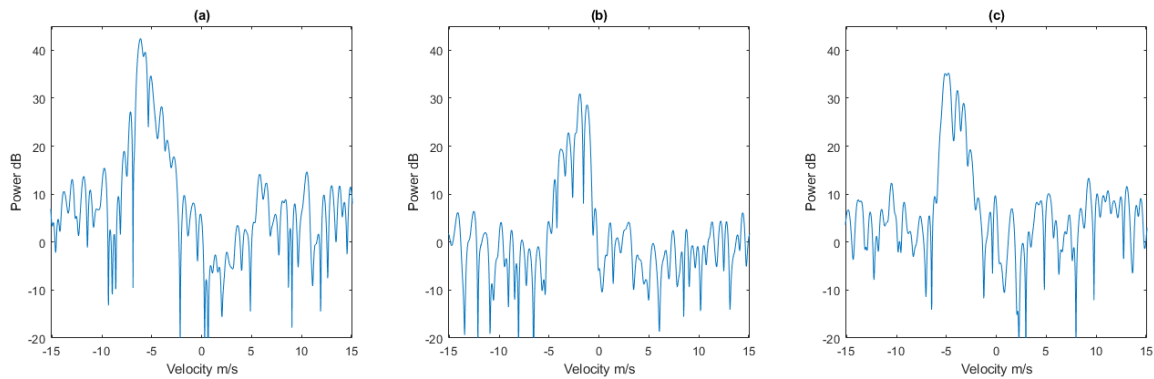


**Figure 20: Doppler spectrum with 2-pulse-canceller added a) ground clutter removed without reducing weather target; b) ground clutter removed with minimal power reduction from clouds; c) the max peak is now weather target**

The 2-pulse canceller worked well with the weather targets, however for point targets, higher order MTI filters, or space-time adaptive filters that take advantages of point target moving speed, may be more preferable. Examples of filter responses of different MTI filter designs are shown in Figure 21.

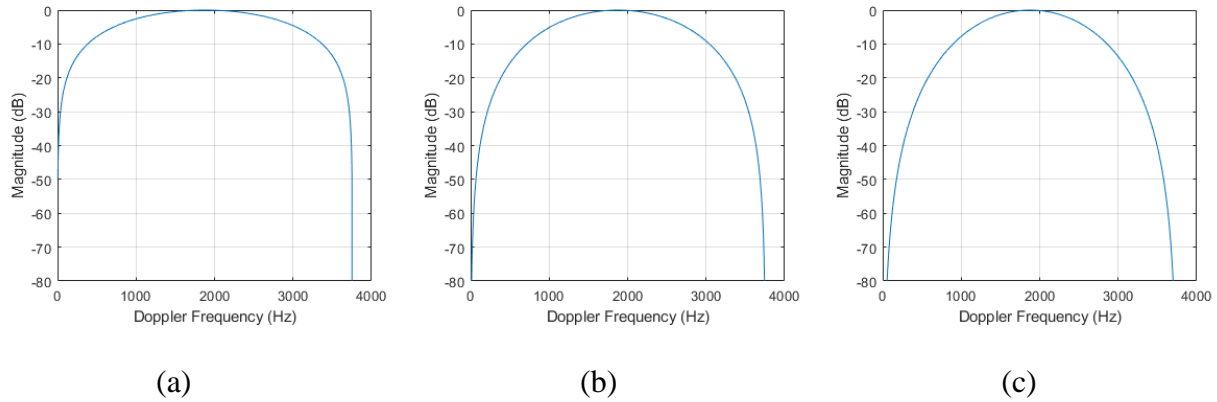


**Figure 21: Normalized MTI Filter response with PRF = 3755 Hz a) 2-pulse canceler; b) 3-pulse canceler; c) filter with transform function  $H(z) = 1 - 3z^{-1} + 3z^{-2} + z^{-3}$**

Since the 2-pulse canceler (Figure 21(a)) has a sharp decent on both sides, it is best for separating weather from ground when the clutter spectrum is shifted and concentrated at zero Doppler. For the 3-pulse filter (as shown in Figure 21 (b)), the power is reduce sooner on either side of the Nyquist frequency. This would affect both the clutter and potentially useful targets (weather). However, the target’s Doppler needs to be inside the pass region of the filter or the filters only hinder the performance.

Besides signal processing, there are a few hardware modifications that would help reduce antenna sidelobe levels. One straight forward modification would be to design a better antenna for the intended application.

Another would be to create a separate channel with an antenna, and a receiver is placed near the main antenna. The sidelobe backscatters would then reach that antenna at different times than the transmitting antenna. Then, using timing logic, an algorithm could be applied to identify and remove ground clutter.

Furthermore, it can be seen in Figure 22 that the ground clutter with near-zero Doppler is suppressed, as described previously. Since in Figure 22(a) there was not high clutter at low velocities, the MTI filter did not contribute as much to the moment data in Figure 22(b).

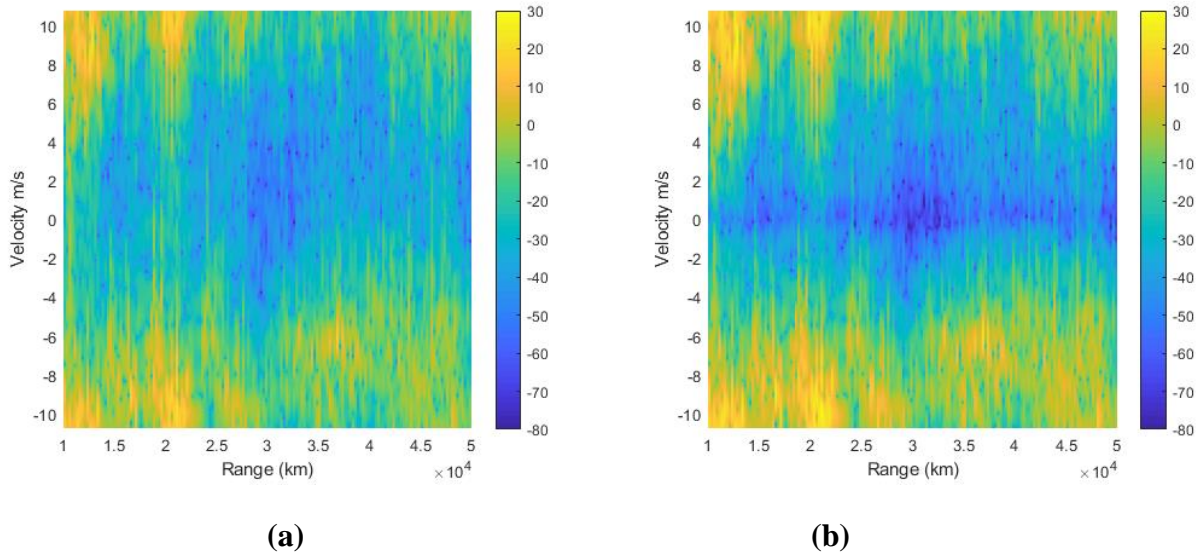


**Figure 22: Range versus Doppler (velocity) plot. (a) is only pulse pair processing. (b) is PPP and MTI with a weather target.**

Another potential problem of the basic AMTI is the “over filtering” problem. It is based on the fact that if the spectral width of the MTI notched filter is too small, there will be significant amount of residue clutter power after filtering. If it is too large, on the other hand, some of the useful target returns (such as weather) will be removed too. This needs to be addressed, especially for airborne scenarios, which motivates the usage of spectrum width of clutter return as part of the AMTI filter designs. A potential method of restoring over filtering was introduced by Golden [23], which essentially “interpolates” the spectrum that is removed by MTI filtering, based on the assumption that the spectrum of the true target (such as weather) has a Gaussian shape.

A more “adaptive” approach, which select the filter responses dynamically, may be beneficial when dealing with varying clutter and signal distributions among different radar resolution cells.

Since there will be different clutters for each bin, having adaptive filters for different clutter spectrum would maximize the usefulness of AMTI filtering. One possible method is choosing a clutter suppression filter based on the clutter's echo power at each range bin [19]. For this approach, two parameters characterizing the clutter spectrum were chosen based on the bandwidth and amplitude of the clutter spectrum power level [19]. The adaptive filters are designed by controlling these two parameters. This method will increase computation load as compared to using a single fixed filter, but it may improve the clutter mitigation and balance the performance of estimating velocities of true targets.

#### **4.4 Adaptive MTI Filtering**

Adaptive MTI filter may improve clutter mitigation while controlling the loss of energy of the weather target. The method proposed applies multiple filters that are pre-designed for different conditions. A specific filter is then chosen out of this list. The next sections will describe the processing and logic behind our adaptive filtering procedure. Based on the estimated clutter power and spectrum width in the radar return.

##### **4.4.1 Algorithm**

Bachmann and Zrnic [24] applied an approach in ground radar that used a filter with an adaptive notch width based on the Gaussian spectrum model. The removed portion of the spectrum was then interpolated after filtering. This method could be applicable to the airborne radar case if there is additional processing after filtering. [24] applied a threshold scaled by the ratio of estimated receiver noise floor level and the receiver spectral noise level. In our approach, there will be two thresholds: one to determine if there is clutter and the second to characterize which filter to use. In this study, we use both power level and spectrum width parameters to determine if the power in the spectrum is caused by clutter returns. Our approach for this study largely adopted the idea in

[24] in terms of threshold level. However, we use two thresholds rather than one, to characterize the MTI filters. We characterize the clutter spectrum using power level and spectrum width and then select a filter based on these two parameters. This approach estimates clutter spectral bandwidth and clutter power level for each range bin. The adaptive MTI filter is basically a notch filter matching the estimated spectral width of the clutter.

One method to determine ground clutter location is the “polar coordinate centroid” method, which identifies the centroid of the clutter spectrum, and applies the designed notched filter based on adaptive adjustment of the clutter spectrum bandwidth [19]. This method has two assumptions that need to be met before this can work. First, it assumes the motion compensation has shifted the centroid of the clutter spectrum to near zero frequency. Second, it assumes the clutter returns have higher power levels than the true targets since it is designed to identify and remove the returns with the highest spectrum peak, which might be instead true weather target in some cases.

Our proposed approach is to pre-design a bank of notch filters that cover the possible clutter spectrums given the radar and flight parameters. There are only a finite number of filters that will be needed for any given clutter power spectrum. These filters are designed and stored, and are applied based on the real-time estimations of the clutter conditions.

This pre-designed filter bank contains a number of frequency-normalized filter coefficients and responses, based on the spectral widths of the clutter, which determines the size of the notched portion of frequency response. For example, suppose that a 1024-point FFT is taken for an arbitrary range bin. The clutter in this range bin is found to have a power level above threshold in 50 consecutive points near zero velocity. A notch filter that blocks these 50 points will be selected for use. This bank will have a set number of frequency normalized filter responses. The filters will

vary based on the spectral width of the clutter and size of the notched portion of the frequency response.

In [23], a high pass filter was used first, then another high pass filter for the other side of the spectrum. To reduce computation, we used a generic band-stop filter instead. An example of a passband for a PRF of 4 kHz is shown in Figure 23. The figure looks like a stopband filter or notch filter, but it is an adapted form of passband. Before the FFT shift, the passband filter is applied. This removes the clutter for both sides of the spectrum.

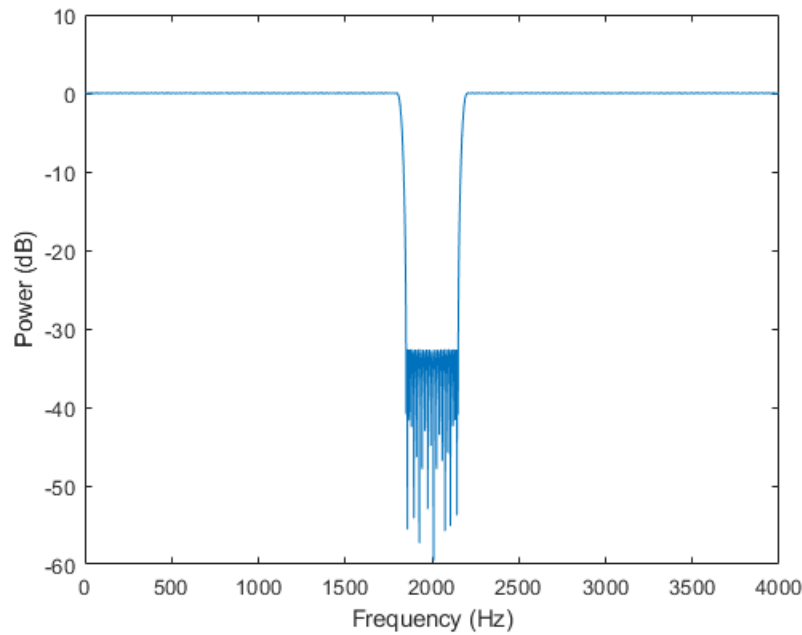


**Figure 23: Band pass filter after the FFT shift is applied to perform clutter suppression in both the negative and positive sides of the spectrum.**

The complete flow chart of the adaptive AMTI filtering solution is depicted in Figure 24. First, we take the FFT of a range bin with a weighted window and zero padding. The FFT will have less spectral leakage with these two additions to the FFT. Secondly, motion compensation must be applied to shift the speed of all the targets back by the speed of the aircraft. The third step is where the logic behind choosing the filter is described.

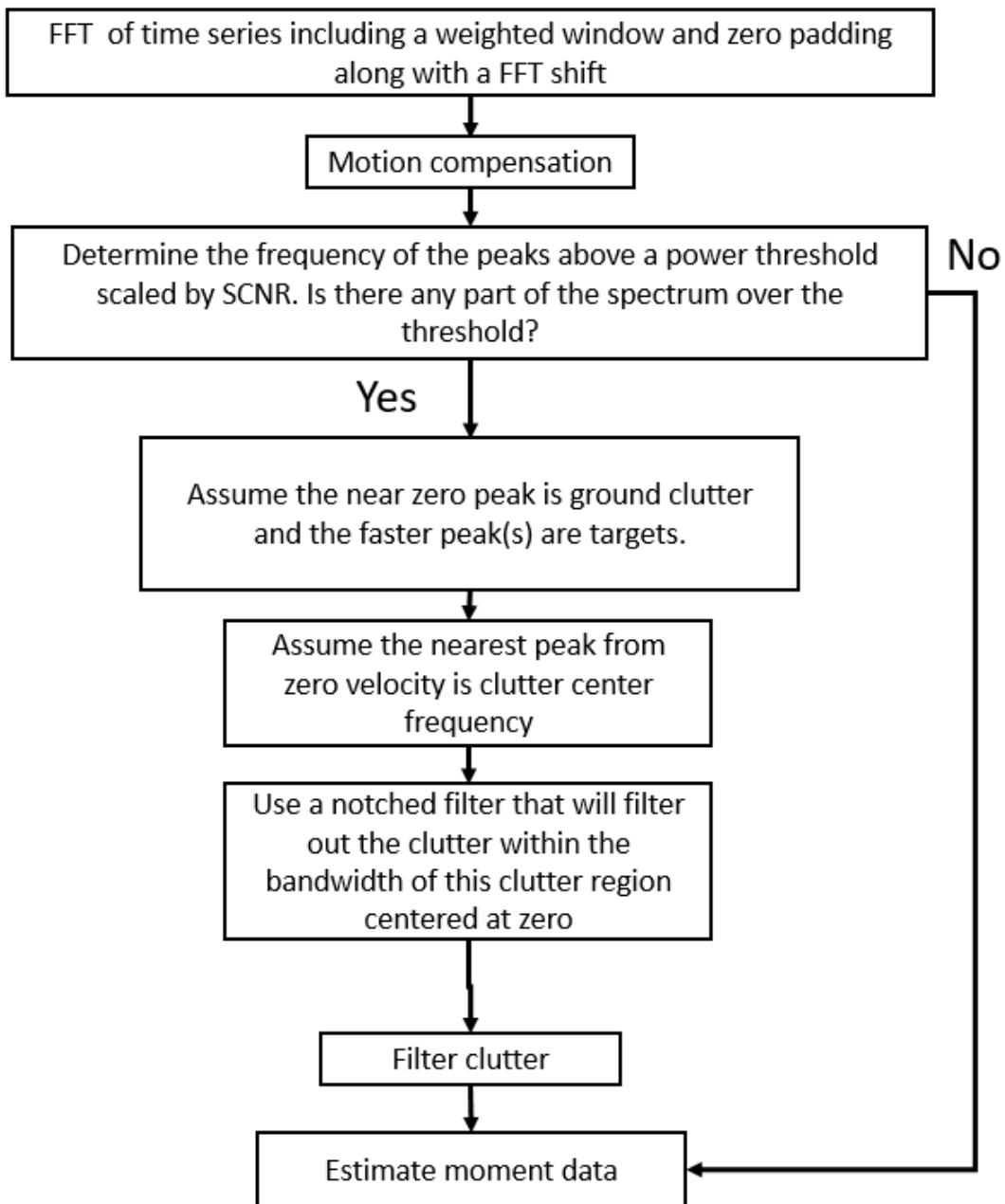


**Figure 24: Diagram of adaptive MTI filter design based on clutter power in range bins and 3-dB clutter bandwidth. This logic is applied to each range bin. A basic power threshold set by the SCNR was used to remove noise or low power clutter.**

Figure 24, a power level threshold is established firstly by choosing a threshold based on the signal plus clutter noise ratio (SCNR) per range bin. For each range bin, if power level of any part of the

spectrum is over the threshold additional logic will apply. If the power is below the threshold, we estimate the weather moment data for that range bin.

We are assuming the ground clutter was shifted correctly to the center of the spectrum by the motion compensation step. Hence, if there is a peak near zero Doppler, we assume it is caused by clutters. A notch filter is selected applied to around zero Doppler, whose bandwidth matches the portion of spectrum span above the power level threshold.

#### 4.4.2 Example Results

Example results for the adaptive MTI filter (whose procedure is explained in the block diagram of Figure 24), for motion-compensated ground clutter are shown in the Figure 25. As can be seen, the selected filter uses correct clutter spectrum width and removes the main portion of the clutter. Note that spectral leakage, which present near positive and negative 5 m/s, are not completely removed. These are relative weak compared to other parts of the spectrum. Compared to the results from basic AMTI such as the range/Doppler plots in Figure 22, on the other hand, it is seen the adaptive filtering result has more “cleaner” clutter mitigation.

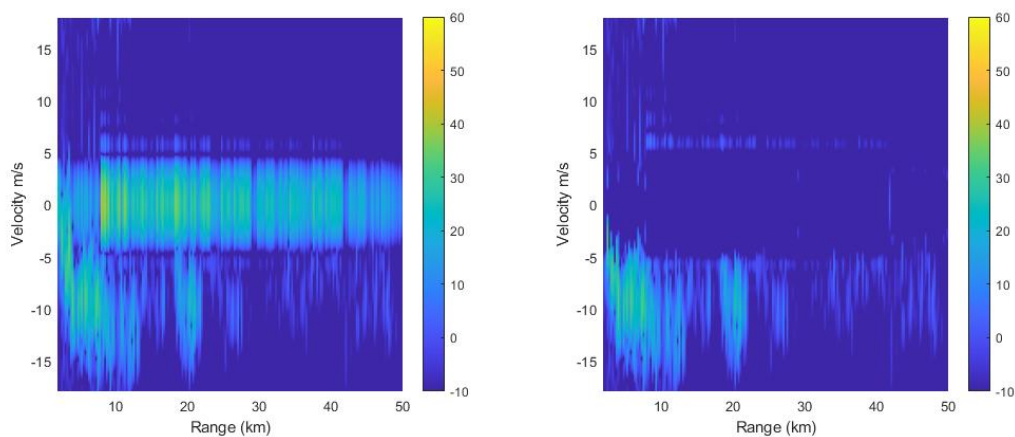


**Figure 25: An example of the adaptive MTI filter results for range-Doppler plot of signal return of a range bin containing weather. (a) weather plus ground clutter. (b) range-Doppler processing result after adaptive MTI filtering.**

For more overlapping cases of ground clutter and weather, a more in-depth tracking algorithm will be needed to keep track of potential over filtering. If there is extremely slow targets this algorithm could remove them as well.

#### 4.5 Detection of Turbulence Hazard through the F-factor Index

The F-factor, which is important to the evaluation of turbulence hazard, is defined as

$$F = \frac{\dot{W}_x}{g} - \frac{W_h}{V_a} [25] \quad (4.18)$$

$F$  = hazard estimate

$W_h$  = Vertical component of wind velocity

$W_x$  = Horizontal component of wind velocity

$\dot{W}_x$  = time rate of change in  $W_x$

$V_a$  = airspeed

$g$  = acceleration of gravity

In equation 4.18 the first part estimates the horizontal effect while the second part estimates the downdraft. When the magnitude of the F-factor reaches greater than 0.13 averaged over a kilometer path the PPI should indicate a hazard. [25] When measuring the first term in equation 4.13, the  $\dot{W}_x$  can be approximated as follows:

$$F_r = \frac{\dot{W}_x}{g} \approx \frac{V_g}{g} \frac{\Delta W_x}{\Delta R} \quad (4.19)$$

$F_r$  = radial component of hazard index

$V_g$  = aircraft ground speed

$\Delta W_x$  = horizontal component of wind velocity

$\Delta R$  = distance between wind speed measurements

In order to get the vertical portion of the wind speed, there must be an estimation by means of conservation of mass. This indirect way is because the radar can only measure radial speed. Since

a forward-looking radar is mostly in the horizontal plane, the vertical component is weak. The downdraft is modeled by:

$$w_h = kh \frac{\Delta W_x}{\Delta R} \quad (4.20)$$

$k = -2$  for performance decreasing shear or  $-1$  for performance increasing shear

$h =$  altitude above ground level ( $h < 250$  m)

Finally, adding this back into the first F-factor equation, equation 4.16 is obtained:

$$F = \frac{\Delta W_x}{\Delta R} \left[ \frac{V_g}{g} - \frac{kh}{V_a} \right] \quad (4.21)$$

Equation 4.16 is valid for altitudes above 250 meters. A least-squares estimation and averaging should be used to reduce the number of false alerts.

The hazard detection equations, information and data came from the American Institute of Aeronautics and Astronautics and their published papers. Gratitude for making this information readily available should be given to them and all other institutes associated with this information such as Research Triangle Institute and NASA-Langley.

## 4.6 Tilt Management

Tilt management of the radar is one of the key methods that pilots use to maximize the return of targets and reducing ground. For SAA/DAA, the radar will sweep in a horizontal plane at a desired tilt angle controlled by the pilot. After pilots get experienced with radars they use more intuition, but before then there are procedures that help the pilot properly angle the radar. One method described below is called threat identification procedure (TIP) [26].

1. Set the bottom edge of antenna beam at 20 NM mark down until touching the ground. Which is easy to tell for the pilot to tell because the edge of the PPI will have much larger returns as the antenna is tilted downward.
2. Next the pilot divides their altitude by two thousand feet while noting the tilt setting.
3. Then add the divided number to the tilt setting to tilt the antenna back up by that number in degrees.

As an example, if a plane is at 14,000 feet above ground level, we tilt the radar down until the PPI is washed out at 20 NM and farther. This will correlate with a downward tilt of about 3.5 degrees depending on the radar elevation beam width (6 degree 3-dB beam width for this case). Then divide the altitude by 2,000 feet and add the number to the tilt which is negative because of the downward point. The new tilt angle is 3.5 degrees upward.

Another distance estimation method is called “the magic radar formula,” which is a basis for all radar tilt management [26]. How to use this method is described as follows: Multiply the nautical miles to the target by 100 then multiply that number by the degrees tilted. This will give the distance up or down the target is relative to the plane in feet. If the target is 10 NM away one degree would result in an estimate of 1,000 feet. This method is used in the height elevation procedure (HEP) to estimate the elevation of a target or echo relative to the aircraft which is describe below [26]

1. Perform TIP and note the degree of tilt,
2. Move the tilt up until the echo of interest is barely visible,
3. Note the new degree of tilt,
4. Use “the magic radar formula” on the difference in degrees of the two tilt measurements,
5. The result is the height of the echo relative to the plane.

These methods are good for quick estimation of the threat levels of weather and other aircrafts for pilots. Nevertheless, implementation of a more autonomous, well-tested algorithm would result in a higher accuracy, constant updating, less human error and better clutter mitigation.

#### **4.7 Overall Processing Chain for an ABSAA Radar Operation**

Airborne sense and avoid (ABSAA) encompasses signal processing as well as tracking and tilt management. As a result, different processing algorithm implementations are required for observing weather and point targets. Since both weather targets and point targets can be estimated well from a linear frequency modulated (LFM) waveform that is the waveform used for our simulations. Figure 26 shows the processing channels for both point target and weather. Both waveforms will go through pulse compression then the processing differs from then on.

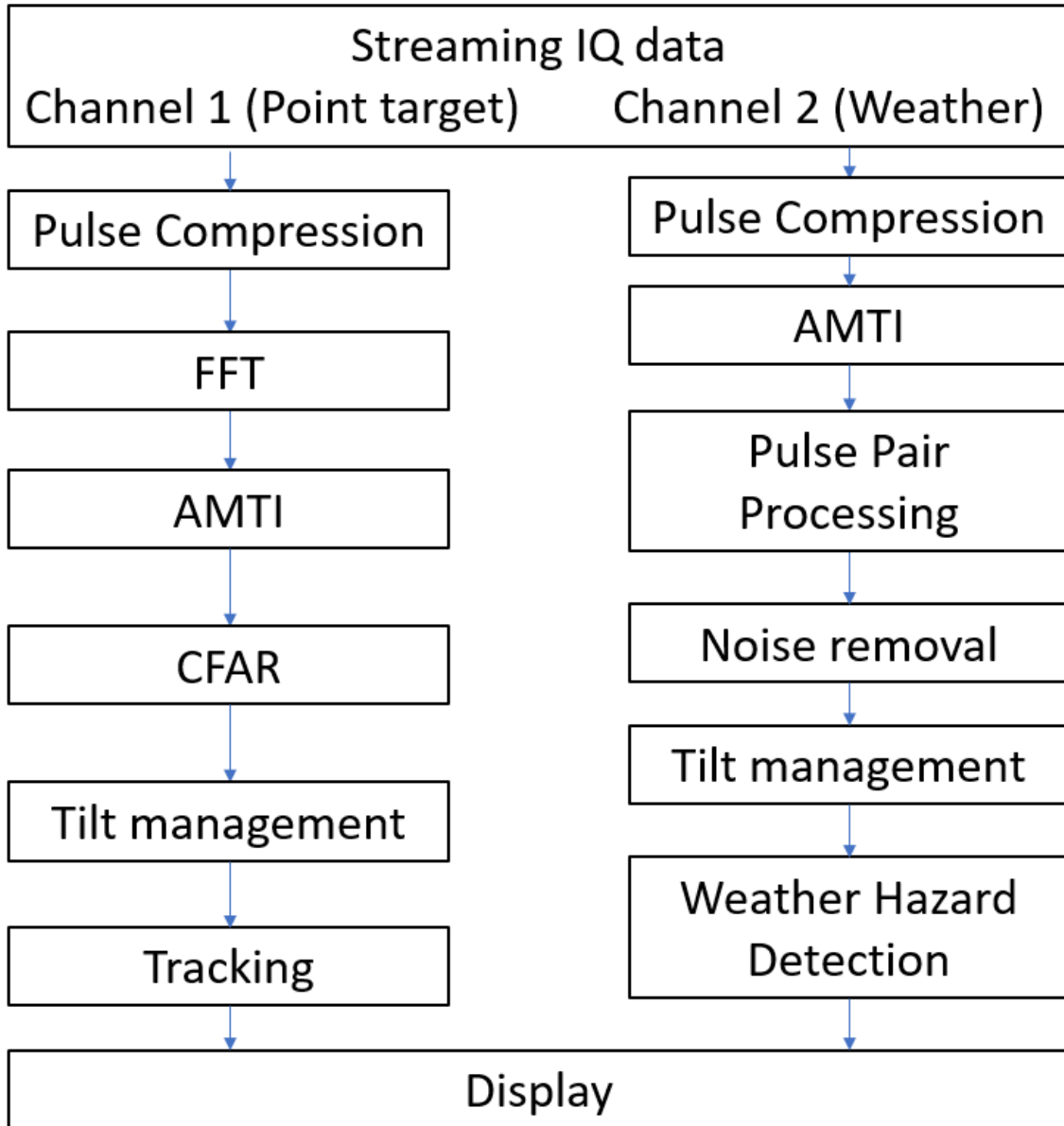


**Figure 26: Summary of the proposed signal processing “chain” for all-weather ABSAA operation. Channel 1 is for point targets and Channel 2 is for weather hazards.**

### **4.7.1 Point Target Channel**

Moving down the point target side, the FFT is taken and the Doppler spectrum is manipulated with an airborne moving target indicator (AMTI). The separation of clutter from targets are more likely in this case with multiple PRF because we expect fast moving targets.

The next block in the point target channel in Figure 26 is constant false alarm rate processing (CFAR). CFAR is used to create a threshold level that estimates the level of noise and uses it for target detection. In our implementation, we use cell averaging CFAR [3]. More complicated CFAR techniques might be advantageous.

Although titled the same, the tilt management of point target and weather target will be different. In the point target case, the airfield will be scanned continuously sweeping at different elevation angles across the front of the airplane.

The last block in this channel, tracking, is not demonstrated in our processing yet, but can be given longer simulation run time. For instance, the PPI can be generated with or without weather as a clutter and populated with targets over many different scans. This would cause much longer computer run times but will be worth it to test tracking algorithms.

### **4.7.2 Weather Target Channel**

For the weather processing channel, note that the AMTI filter is different for the point target. As weather usually moves slower than point targets, they appear closer to the zero Doppler frequency. The filtering is lumped into this block. The adaptive filtering is applied as shown in the block diagram from Figure 24 which lead to PPP.

After MTI filtering, pulse pair processing (PPP) was applied in the weather processing channel to estimate the radial velocity and spectrum width. Noise removal is currently implemented as simple thresholding while more advanced algorithms are available to estimate and adjust the threshold based on noise.

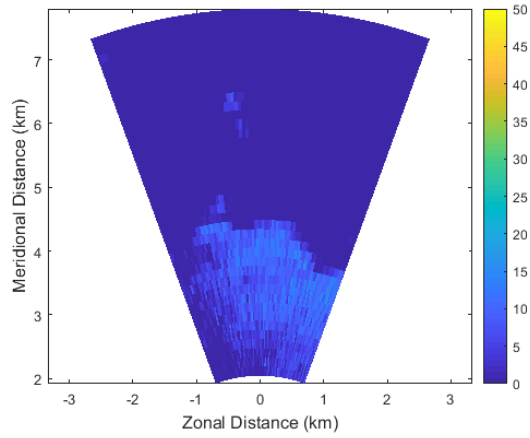
Weather hazard detection is estimated by calculating the F-factor along with the reflectivity. It uses the conservation of mass paired with the radial velocity measurement to predict the updraft or downdraft [25]. Even though there are updraft/downdraft estimations, to be safe it would be best to avoid any higher reflectivity levels. This would mean flying around any weather above a certain reflectivity. Depending on the operation of the radar, the weather could also be tracked instead of only avoided.

Storm tracking is achieved using a radar methodology called Thunderstorm Identification, Tracking, Analysis and Nowcasting (TITAN) [27]. TITAN uses digital image processing and thresholding to break the PPI into blobs or weather cells. The thresholding ranges from 15 dBZ to 50 dBZ and is broken up into 4 tiers: snow bands (15-25 dBZ), mesoscale convective complexes (25-35 dBZ), convective storms (30-40 dBZ) and individual convective cells (40-50 dBZ) [27]. Another threshold is needed for the volume size of the weather cell. Then the TITAN method follows simple rules to determine which cloud coverage has merged or split depending on predicted pathing, storm characteristic set, and location.

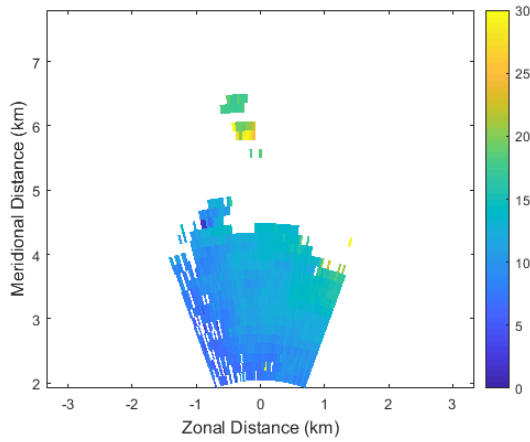
#### **4.7.3 Results for NASA flight test data**

The AMTI processing results in improved reflectivity (or power) measurement, as shown in Figures 27(a – d). For the radial velocity and spectral width, the majority of power return from the

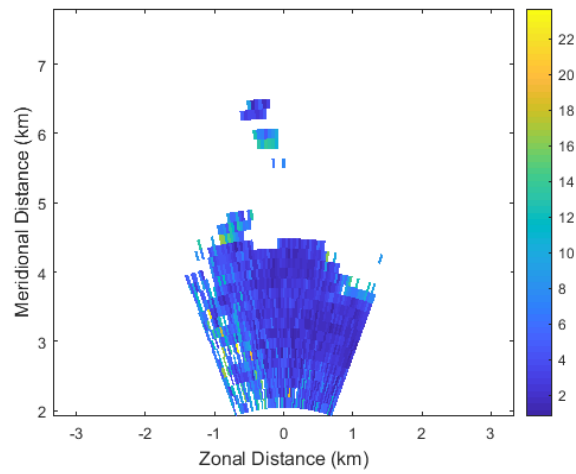
ground was removed. As a result, the radar resolution cells containing clutter appear to be noise-like, and thus they were removed from the PPI scan result with thresholding as mentioned before.



(a)



(b)



(c)

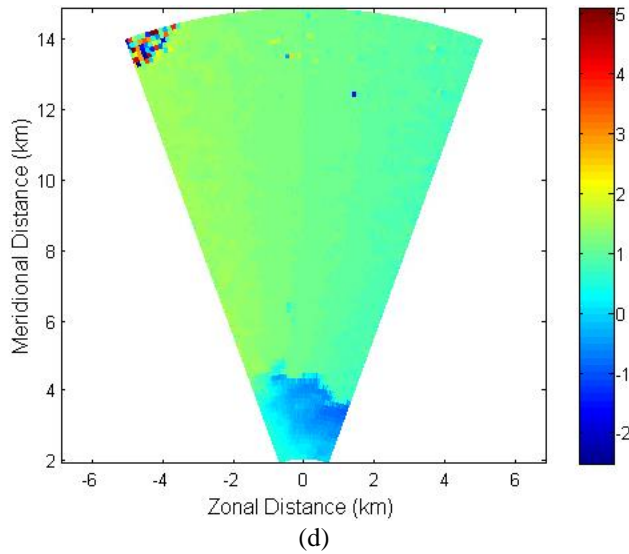


**Figure 27: Airborne radar scan simulation using NASA Langley’s flight test data as truth field. The simulation implemented part of the channel 2 chain in Figure 26 with F-factor added in. The plots are (a) reflectivity (dBZ), (b) velocity measurement (m/s), (c) spectral width (d) The F-factor for updrafts/downdrafts.**

#### 4.8 Motivation and Basic Configuration of Simulation Using NEXRAD Data as Truth

##### Input Field

The airborne radar measurement provided by NASA flight test has been used as our main source of “truth data” in the simulator. It has certain limitations, however, due to limited variability of weather scenarios. Another important source of truth data is the NEXRAD measurements from NOAA. Although the datasets are measured from ground radar, it can be re-processed to construct airborne-equivalent truths for all six polarimetric radar variables of weather events, and it is widely available since the NEXRAD network has coverage of the entire country. Therefore, we also used the NEXRAD cases in our airborne radar simulations.

The data from NEXRAD is reverted back into back scatterers as IQ data. A covariance matrix-based method is applied to the time series to revert the back scatterers [5]. In turn, this makes each cell in the area of interest a “target” with weather moment information.

Once the IQ data is generated, the simulation uses a time-domain system to update the electronic behavior models for the antenna, transmit/receive modules, platform and pulse compression waveforms [5]. Also, the degradation from ground clutters are included at this step. The new IQ data that has been adapted to airborne characteristics can now be used to test radar signal processing.

The example we studied below is based on a tropical storm in Texas called Imelda in 2019. A portion of the storm is shown from a NEXRAD radar scan in Figure 28(a). A single scan from NEXRAD’s VCP (volume coverage pattern) is used. This is a simplified approach, since a more sophisticated simulation will resample the 3D volume to generate CAPPI (constant altitude PPI) truth fields. The scan from NEXRAD is treated as the “correct” measurement or the “truth”. Figure 28(b) shows how the NASA radar would perform with the same backscatters and additional ground clutters.

For the simulation in Figure 28, the azimuth size was 12 degrees, and the scan range was from 2 km to 20 km with a two-pulse CPI. The area chosen and the amount of pulses were limited because of computation time. The performance of the simulated radar is hindered by only having two pulses in a CPI and is less comparable to actual systems. The rest of the system parameters and geometry are the same as those listed in Table 1.

**Table 3: “Default” Airborne Radar Simulation Parameters for Section 4.8**

<b>Parameter</b>	<b>Values</b>
Pulses per CPI	2
Operating frequency	9.3 GHz
Noise figure	4 dB
PRF	1500 Hz
Pulse width	10.8 $\mu$ s

Waveform	Barker code 13
Antenna Gain	30 dB
Flight altitude	5000
Aircraft speed	100m/s (assuming motion compensation is done so the spectrum is set to centered around zero frequency)
Clutter type	Flat Ground

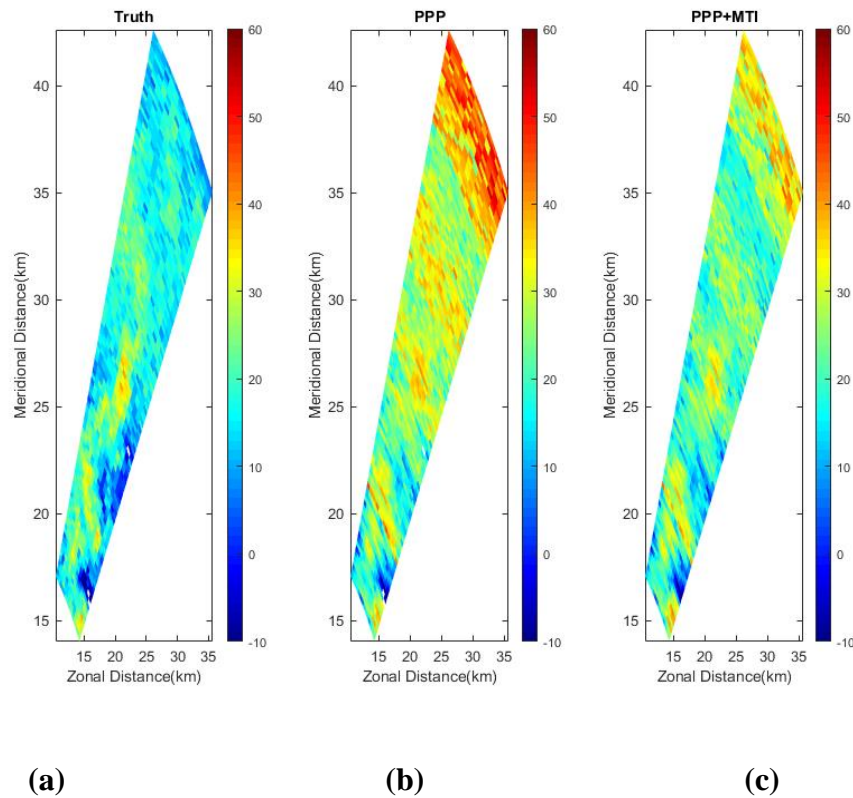


**Figure 28: Sample PPI scan of reflectivity estimation using NEXRAD weather radar truth data. The radar system parameters are listed in Table 1. (a) NEXRAD’s reflectivity measurement data, which is treated as the truth weather field. (b) Simulated representation of the NASA radar recording of the same event with PPP. (c) Simulated data with PPP and MTI processing.**

Figure 28 (b) shows the simulated airborne weather scan with clutters added in. The same clutter generator as in the previous sections are used. The clutter setting is as follows: depression angle was 5; altitude was 5000 meters; clutter was scaled with a coefficient of  $10^6$ ; clutter type was flatland. The clutter was scaled up to reveal what could have been the case for worse conditions.

Figure 28(c) shows the results of applying the basic AMTI filtering. As is shown in the scan result, the simple two-pulse clutter canceller has made some improvements. Some areas have up to an improvement factor of 19 dB for portions of the scan.

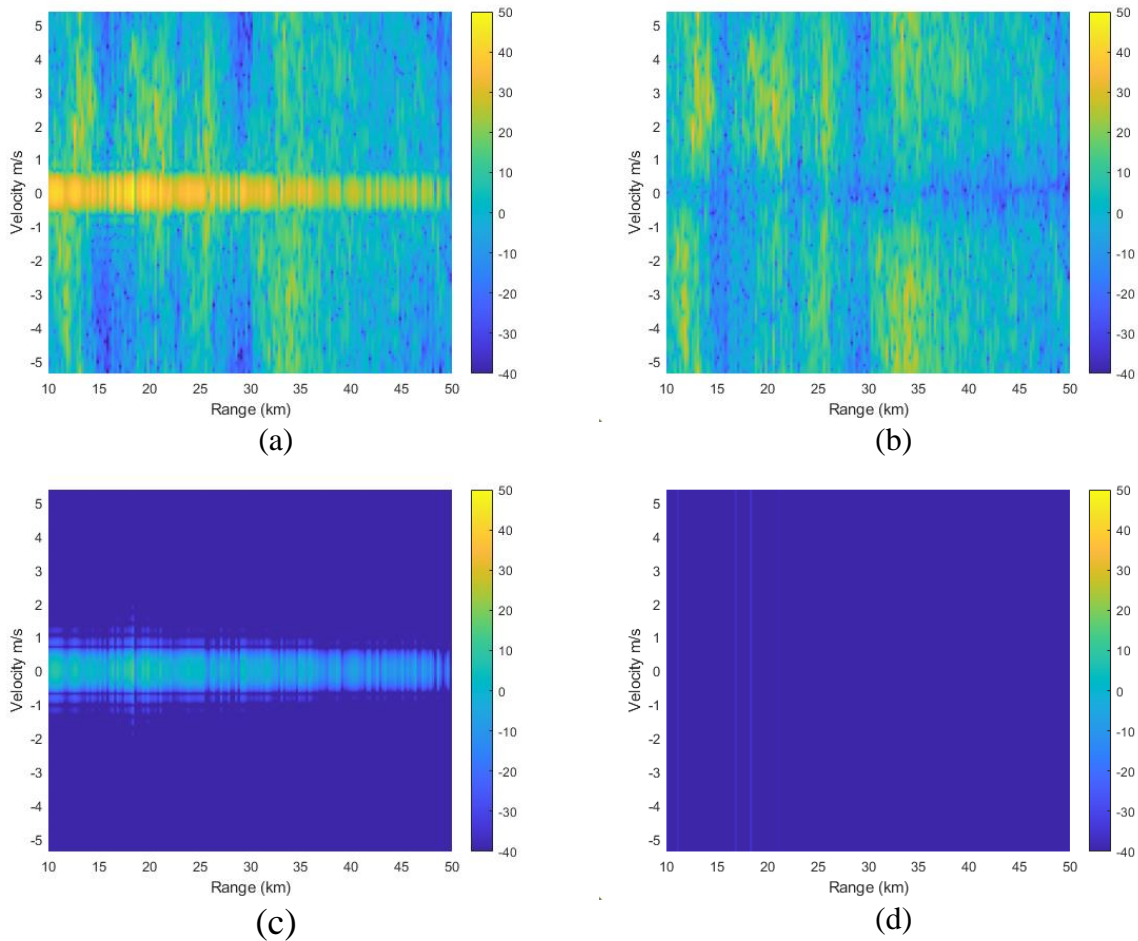


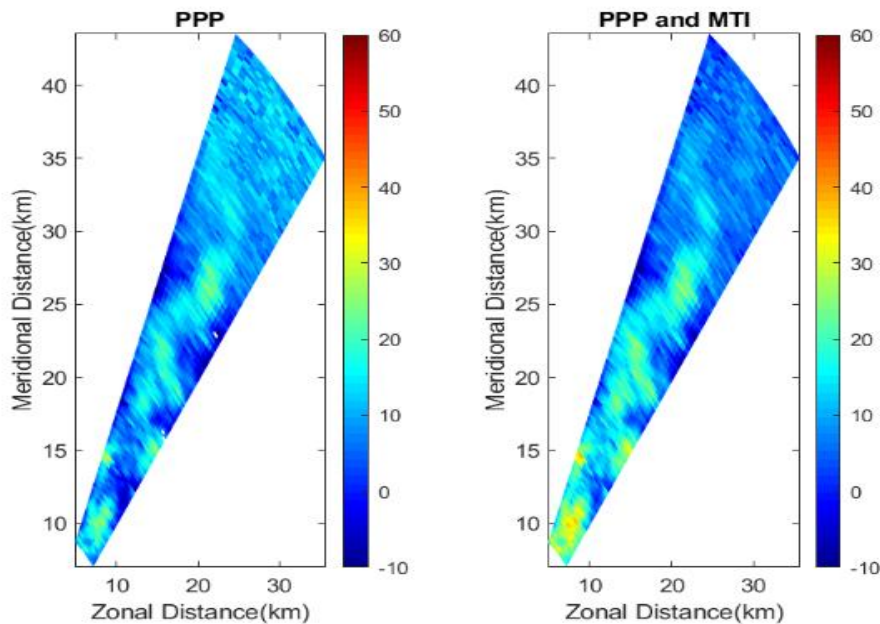
**Figure 29: PSD of weather and ground clutter. The parameters are the same as in table 3. (a) the spectrum of weather with simulated ground clutter at altitude of 400 meters. (b) MTI applied to (a). (c) A look at the simulated ground clutter. (d) The ground clutter spectrum with a MTI filter.**

#### **4.8.1 Evaluation of Impacts of Different Parameters**

Now we can create various scenarios by changing some of the system and environment parameters, and investigate how the performance in terms of standard deviation (STD) from truth and clutter Improvement Factor (IF) from results of MTI processing under these different scenarios.

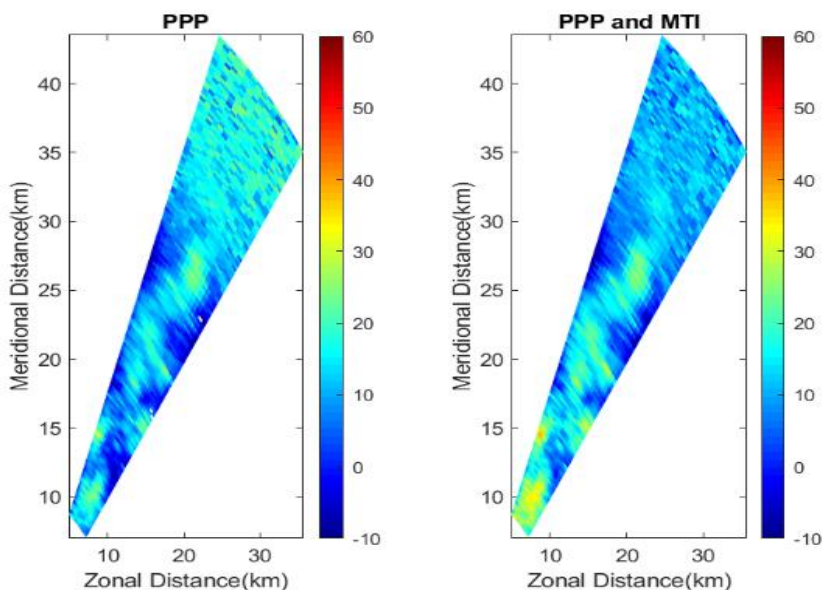
#### **4.8.2 Impact of Clutter Power Levels**

In this section, we used the airborne radar system and flight geometry parameters listed in Table 3 for different clutter strength levels. The clutter strength level is characterized as a “clutter scale factor”, which is simply a scale applied to the minimum (or default) clutter return levels. To simplify the processing, the aircraft speed is set to zero (equivalently, assuming the motion compensation has been implemented). The Signal to Clutter Ratio (SCR) varies from 14 to 44 to by changing the clutter power scaling factor from 70 to 100 dB. The results for simulations including clutter are illustrated in Figure 30.



(a)

(b)



(c)

(d)

**Figure 30: Effect of the two-pulse AMTI canceller on the simulated weather scan using NEXRAD truth data for the similar airborne radar case. The strength of ground clutter is adjusted to different levels. The left column is the weather radar scan result with PPP, the right column is the result after AMTI. Each row contains the results for a clutter strength level. (a) and (b) have a clutter scale factor is  $6.4e7$ . (c) and (d) have a clutter scale factor is  $6.3e8$ .**

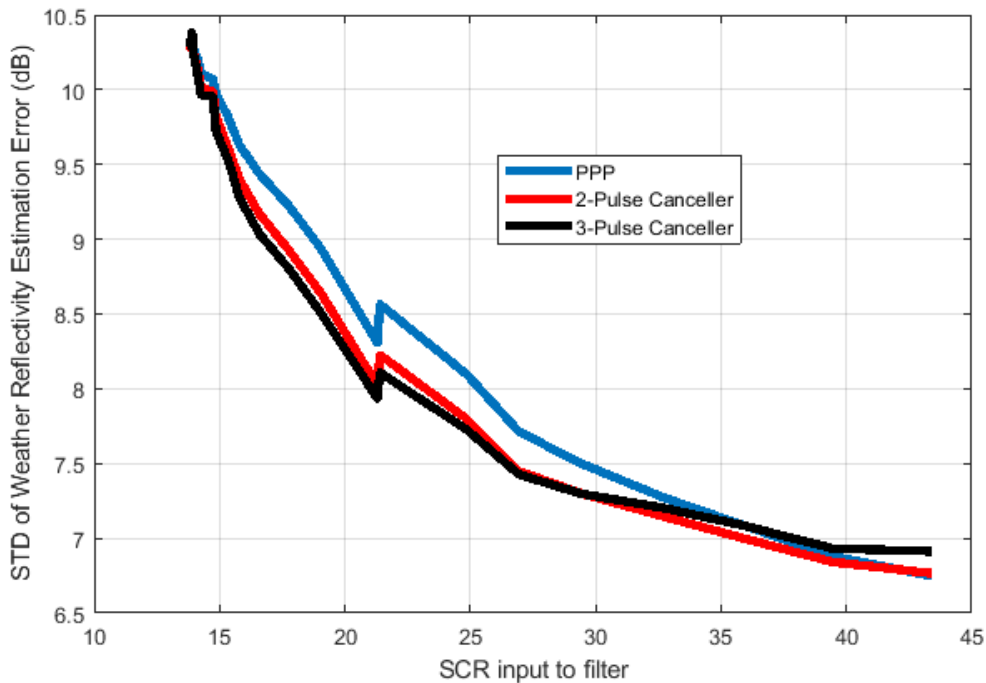


**Figure 31: The improvement of clutter mitigation using the two-pulse and three-pulse canceller, for different clutter strength levels. The ground clutter was flat ground. The performance is measured using standard deviation (STD) of errors compared to the truth scan data versus the signal to clutter ratio for the input of the cancelers.**

Comparing Figure 30(a) with (b), at a certain range, the quality of the reflectivity estimation is unusable, even when AMTI is applied. This is mainly because that distinguishing between the clutter and weather is increasingly difficult at locations where weather is intermittent. Even so, there is a noticeable improvement from the MTI result.

Figure 31 shows standard deviation (STD) of reflectivity estimation vs Signal to Clutter Ratio (SCR) at inputs of MTI filters. The comparison is between the ideal original data from NEXRAD and either processing with PPP or AMTI. The 3-pulse canceler and the 2-pulse canceler were tested as well. The higher the standard deviation from the ideal the worse the prediction. The 3-pulse

canceler did worse at the lower levels of ground clutter. However, unlike the 2-pulse canceler, this filter response amplifies a region of the Doppler spectrum where there should not be any ground clutter. Therefore the filter is increasing the reflectivity from the weather targets or a point target. From an operational standpoint this is not a problem since a pilot will just avoid the weather in general.

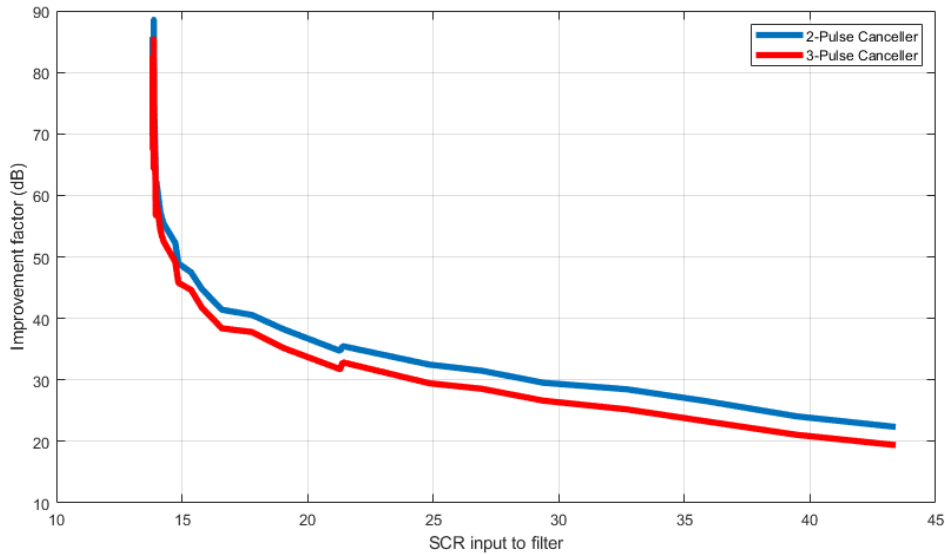


**Figure 32: The plot shows the improvement factor (IF) versus the SCR to the input of the MTI filter. The performance is quantified from the Improvement factor from equation (4.7). The parameters were the same as table 3 with the altitude changed to 400 meters and the clutter was scaled up by 70 dB to 100 dB to show how well the filters work in extreme conditions.**

Figure 32 shows that the improvement factor are in range of 20 to 90 dB. It is important to show the STD and the improvement factor because the filter is able to remove all the clutter at lower SCR. When comparing Figure 31 to Figure 32, the STD shows the PPI scan data quality degrades at a certain point. It is easier to see this qualitatively in Figure (a)-(d).

## **Chapter 5: Summary, Conclusions, and Future Work**

---

### **5.1 Summary**

In this thesis, we started the discussions of fundamental radar theory, hardware and systems. We stated the goal of this work as improving the basic SAA/DAA type of airborne radar operations in presence of ground clutter.

Clutter was modeled using the constant gamma clutter model in MATLAB's phased array system toolbox. The clutter was then added to data from NASA's airborne radar flight campaigns. In order to simulate different flight observation scenarios with the same data, the vertical cloud distribution was estimated and incorporated.

An overview of different airborne radar related processing techniques were discussed, including the algorithms for both weather and point targets. Some topics discussed were motion compensation, AMTI, Adaptive filtering, PPP, multi-lag, and turbulence hazard observation.

Using the block diagram in Figure 26, the NASA airborne data with some processing and simulated ground clutter was processed. To expand on testing the algorithms, MATLAB simulation system was used again. The airborne radar simulator was used to evaluate MTI improvement factors and the standard deviation from "truth data" with different levels of ground clutter degradations.

### **5.2 Conclusion**

The main objective was to accurately model ground clutter for SAA/DAA airborne radars and to test algorithms that can be applied to commercial airborne radars. In order to achieve this, the constant gamma clutter model was applied to real airborne data as well as simulated data with various scenarios and platform trajectories. A brief overview of multiple algorithms for the entire processing chain for weather and point targets were discussed. Not all the algorithms introduced

were tested, though. The ones that were tested showed significant improvement to the PPI and functionality of the radar.

The adaptive filtering technique described here showed that it could significantly reduce the ground clutter levels. More rigorous testing should be used on the filtering technique to remove any potential problems, either removing too much or removing too little of the PSD. Fortunately, the data from NEXRAD and the simulation strategy give nearly unlimited resources to generate different test scenarios.

### **5.3 Future Work**

Since the simulator discussed in this paper can generate different scenarios the more scenarios the better. Generating an in depth bank of different saved backscatterers for a given radar would be ideal for testing different algorithms. Hence expanding the scenarios is constant source of future work.

In terms of algorithms, there are a few algorithms that should be expanded upon and tested, such as:

- Using tilt management to maximize the power return from the core of storms
- More complicated staggered PRF algorithm
- A more reliable turbulence prediction method
- Tracking for long scan times for both weather and point targets

Also, phased array radars are becoming cheaper, so commercial use of these types of radars is increasing. Therefore, a more in-depth look into STAP would be a good investment for the future.

A few problems arise from the simulator that should be addressed. First, The blind range is limited to the blind range of NEXRAD, so there is minimum pulse width limit. Second, developing a simulator use three-dimensional NEXRAD data would be ideal because then the simulator will not need to estimate moment values at different elevations. Finally, the simulation takes an extreme amount of time, so smaller areas of interest and less pulses were demonstrated here. Decreasing the run time will greatly help with simulating more pulses, large scanning and longer scan times for SAA/DAA.

## References

- [1] W. A. Lies, L. Narula, P. A. Iannucci and T. E. Humphreys, "Low SWaP-C Radar for Urban Air Mobility," in *2000 IEEE/ION Position, Location and Navigation Symposium (PLANS)*, Portland, OR, USA, 2020, pp. 74-80, doi: 10.1109/PLANS46316.2020.9110148..
- [2] R. Nepal, *Advanced signal processing for multi-mission airborne radar*, 2018.
- [3] G. M. Harkness , *Airborne Pulse Doppler Radar*, Artech House INC., 1996.
- [4] B. R. Mahafza, *Radar Signal Analysis and Processing Using MATLAB*, Taylor Francis Group, LLC, 2009.
- [5] Z. Li, "Phased Array Radar System Simulator (PASIM): Development and Simulation Result Assessment," in *Remote Sensing*, 2019.
- [6] National Instruments, *Understanding FFTs and Windowing*.
- [7] M. Mathe, "DSP Illustrations," [Online]. Available:  
<https://dspillustrations.com/pages/posts/introduction/welcome-to-dspillustrationscom.html>.  
[Accessed 23 September 2020].
- [8] MATLAB, "mathworks.com," MATLAB, [Online]. Available:  
<https://www.mathworks.com/help/phased/ref/phased.constantgammaclutter-system-object.html>.
- [9] M. Diani, G. Corsini, F. Berizzi and D. Calugi, "Ground Clutter Model for Airborne MPRF Radars in Look-Down Search Mode," *IEE Proc.-Radar*, vol. Vol. 143, no. No. 2, 1996.

- [10] S. Harrah, E. Bracalente, P. Schaffner and C. Britt, "NASA's Airborne Doppler Radar for Detection of Hazardous Wind Shear: Development and Flight Testing," NASA Langley Research Center, 1993.
- [11] MathWorks, "Gaussian Models," [Online]. Available: <https://www.mathworks.com/help/curvefit/gaussian.html>. [Accessed 11 February 2020].
- [12] J. H. collis and SM, "Py-ART," JORS, 2016. [Online]. Available: <https://arm-doe.github.io/pyart/>. [Accessed 25 February 2020].
- [13] C. Schleher, MTI and Pulsed Doppler Radar with MATLAB Second Edition, Norwood: Artech House, 2010.
- [14] M. Skolnik, Radar Handbook second Edition, McGraw-Hill, 1990.
- [15] Y.-K. Kwag, C. Min-Su and J. Chul-Ho , "An Adaptive Compensation of Moving Clutter Doppler Shift for Helicopter MTD Radar," in *2006 CIE International Conference on Radar*, Shanghai, 2006.
- [16] G. A. Andrews, "Airborne Radar Motion Compensation Techniques," Naval Research Laboratory , D. C., 1972.
- [17] M. A. Richards, Fundamentals of Radar Signal Processing, McGraw Hill Education, 2014.
- [18] L. Lei, G. Zhang, R. D. Palmer, B. L. Cheong and Q. Cao, "A Multi-lag Correlation Estimator for Polarimetric Radar Variables in the Presence of Noise".
- [19] W. Renbiao, H. Yanfei and L. Hai, "Adaptive Ground Clutter Suppression for Airborne Weather Radar Based on Echoes Power," Tianjin Key Laboratory for Advanced Signal Processing, Tianjin, China.

- [20] C. Wolff, "Radartutorial.eu," [Online]. Available:  
<https://www.radartutorial.eu/06.antennas/an36.en.html>. [Accessed 23 September 2020].
- [21] MATLAB, "MathWorks," [Online]. Available:  
<https://www.mathworks.com/help/phased/examples/ground-clutter-mitigation-with-moving-target-indication-mti-radar.html>. [Accessed 21 July 2020].
- [22] M. Arbabian, M. Bastani and M. Tabesh, "Optimization of PRF Staggering in MTI Radar".
- [23] J. Golden, "Clutter Mitigation in Weather Radar Systems Filter Design and Analysis," Swarthmore College Engineering Department, Swarthmore, PA.
- [24] M. S. Bachmann and S. D. Zrnich, "Suppression of Clutter Residue in Weather Radar Reveals Birds' Corridors Over Urban Area," *IEEE Geoscience and Remote Sensing Letters*, vol. 5, no. 2, pp. 128-132, 2008.
- [25] C. L. Britt, S. Harrah and L. H. Crittenden, "Microburst Hazard Detection Performance of the NASA Experimental Windshear Radar System," American Institute of Aeronautics and Astronautics, Washington D.C., 1993.
- [26] A. Trammell, "Antenna Tilt: The Key Radar Control," theairlinepilots, [Online]. Available:  
<https://www.theairlinepilots.com/forumarchive/aviation-weather/wx-radar-antenna-tilt.pdf>. [Accessed 10 October 2019].
- [27] M. Dixon and G. Wiener, "TITAN: Thunderstorm Identification, Tracking, Analysis, and Nowcasting - A Radar-based Methodology," National Center for Atmospheric Research, Boulder, Colorado, 1992.
- [28] RTCA, "Minimum Operational Performance Standards (MOPS) for Airborne Weather Radar Systems," RTCA, 2016.

- [29] N. Goodman, *Radar Signal Processing Notes*, Norman, 2019.
- [30] C. Maklin, "Medium," 29 December 2019. [Online]. Available:  
<https://towardsdatascience.com/fast-fourier-transform-937926e591cb>. [Accessed 7  
February 2020].
- [31] L. Lei, G. Zhang, R. D. Palmer, B. L. Cheong and Q. Cao, "A Multi-lag Correclation Estimator for Polarimetric Radar Variables in the Presence of Noise," University of Oklahoma, Norman, 2019.
- [32] M. Arbabian, M. Bastani and M. Tabesh, "Optimization of PRF Staggering in MTI Radar," 2005.